A Petrographic and Geochemical Characterization of Magnetite Ore at the Island Queen Skarn, Puerto Rico

By

Samantha VanDenburgh

A thesis submitted to the Graduate Faculty of
Auburn University
in partial fulfillment of the
requirements for the degree of Master of Science

Auburn, Alabama
May 10, 2025

Approved by:

Laura D. Bilenker, Chair, Assistant Professor, Department of Geosciences
Raphaël Gottardi, Associate Professor, Department of Geosciences
Thomas Hudgins, Professor, Department of Geology, University of Puerto Rico, Mayagüez

Abstract

Skarns classically form as the result of a multi-stage process including magmatic intrusion, alteration of carbonate-rich host rock, metasomatism, and later introduction of meteoric fluids. These processes transfer and concentrate metals like iron (Fe) into economic deposits. Puerto Rico serves as a natural laboratory to characterize mass transfer across Fe skarns. It is an extinct, unaccreted island arc and has a mining ban, leaving the outcrops available for study with minimal destruction. This research takes advantage of this opportunity to study Fe transport and deposition through fieldwork, petrography, and geochemical analyses of the Island Queen skarn.

At Island Queen, magnetite ore partially replaces limestone lenses hosted within volcaniclastics. Seventeen samples were analyzed including Fe oxide ore, limestone host rock with varying degrees of replacement, and weakly magnetic volcaniclastics. Petrography revealed predominantly magnetite, frequently with martite rims and evidence of dissolution-reprecipitation, and minor hematite, garnet, quartz, and chlorite. Elemental concentrations were measured in the ore, and electron images and X-ray maps revealed zoning in the magnetite that reflects changes in the ore-forming fluid. The Fe and oxygen (O) isotope compositions of the magnetite and host rocks indicate a dominant meteoric component in the fluid(s) that transported Fe and/or later altered the magnetite.

Acknowledgments

I would first like to express my gratitude towards my advisor, Dr. Laura Bilenker. Your dedication to your students has contributed to both my academic success and professional development. I would also like to thank my collaborators at the University of Puerto Rico, Mayagüez, namely Dr. Thomas Hudgins. Thank you for your mentorship and the extensive field knowledge you have provided to me. This research has been made possible through the collaboration and support of those around me, I would like to extend my most sincere gratitude to everyone who has contributed. Thank you to those who conducted early field work and sample collection: David Giovannetti-Nazario, Marisa Barefoot, and Anabel Collazo Irizarry. Dr. Zeki Billor at Auburn University with LA-ICP-MS, and Dr. Lowell Moore at Virginia Tech with EPMA for their expertise and instrumentation guidance. The personnel of the University of British Columbia PCIGR facilities, especially Kathy Gordon and Dave Daquioag for support with sample preparation and Fe isotope analysis. Dr. Ilya Bindeman at the University of Oregon for collecting oxygen isotope data for this project. Elyssa Rivera for her assistance in isotope preparation and data collection, as well as all of the support and guidance she has given me along the way. The undergraduate students for assisting with isotope preparation and petrography: Jake Swartz, Asher Staubach, and Caroline Locker. Dr. Raphaël Gottardi for providing microscope and thin section scanner access, as well as feedback and input as a committee member. The Economic Geology and Geochemistry Group and the friends here at Auburn for all their feedback and support. The funding sources that have made this project and conference travel possible: NSF (EAR-2217927 & EAR-2217928), the Auburn Geosciences Advisory Board Travel and Student Research Grants, the GSA SE Section Travel Grant, and the Auburn Going Places with Geosciences Grant. Lastly, I would like to thank my family for always providing support and encouragement throughout my academic journey.

Table of Contents

List of Figures

List of Tables

1. Introduction

Iron (Fe) is a critical resource for all facets of modern life. Most Fe ore mined globally is used in steel, which is required for infrastructure, transportation, appliances, and mechanical equipment. Steel is particularly important in the transition to green energy, as it is the main component in wind turbines and is used in solar panel structures (Wilburn, 2011; Cooperman, 2023). As the global population continues to grow and more infrastructure is required, locating more Fe ore deposits is crucial.

Puerto Rico serves as a key location for conducting Fe ore research for two main reasons. First, there is an active mining ban in place in Puerto Rico, but historically, the Island Queen Mine and Keystone Mine produced a combined 220,000 tons of Fe ore (Vazques, 1960; Bawiec et al., 1999). This limited mining activity provides an opportunity to revisit exposed ore deposits decades later. Second, Puerto Rico is an extinct island arc that remains unaccreted (Bawiec, 1998; Jolly et al., 1998; Schellekens, 1998). Therefore, the complex geological history that produced a wide variety of metal deposits across the main island has been well-preserved.

This research characterizes the Island Queen Fe skarn in Puerto Rico by defining the origin and composition of the Fe ore (magnetite), source(s) of fluid, extent of fluid rock interactions, and access to the skarn outcrop in the field. With the completion of this project, the three skarn deposits (Island Queen, Keystone, Tibes) targeted by a larger research effort are now fully characterized allowing for the strategic, detailed comparison of magmatic-hydrothermal systems across Puerto Rico. This exceptional opportunity to study an unaccreted Fe skarn contributes to our understanding of Fe transport and deposition in magmatic-hydrothermal systems.

2. Background

2.1. Geologic overview of Puerto Rico

Puerto Rico is a Caribbean island located at the eastern end of the Greater Antilles. The island itself is located on the Puerto Rico-Virgin Islands (PRVI) microplate situated at the boundary of the Caribbean-North American plate (Figure 1) (Schellekens, 1998). Puerto Rico is separated into three geologic provinces known as the Southwestern Igneous Province (SIP), Central Igneous Province (CIP), and Northeastern Igneous Province (NIP) (Schellekens et al., 1991; Schellekens, 1998; Bawiec et al., 2001). These provinces are defined by lithology as well as fault boundaries, and all of them experienced iterations of faulting and magmatic intrusions (Schellekens et al., 1991; Schellekens, 1998); a detailed map of the geologic formations and fault traces from Jolly et al. (1998) is provided in Appendix A. The tectonic and magmatic history of Puerto Rico resulted in the ideal environments for metal transport and deposition.

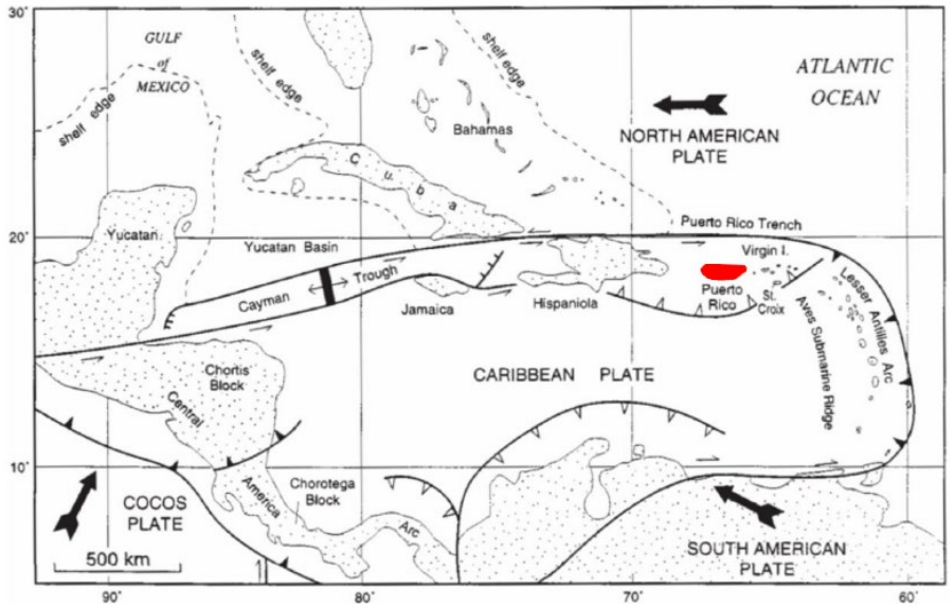

Figure 1. Tectonic map of the Caribbean (modified after Lidiak and Larue, 1998).

2.2. Skarn formation

Skarns can form in various tectonic settings and are defined generally by their mineralogy and main commodity (e.g., Einaudi et al., 1981; Meinert et al., 2005 and references therein). They are mined for metals including Fe, molybdenum (Mo), tungsten (W), gold (Au), copper (Cu), zinc (Zn), and tin (Sn) (Einaudi et al., 1981; Meinert et al., 2005; Robb, 2005). The simplified model of skarn formation is traditionally considered to be the result of a three-stage process. First, a magmatic intrusion enters a permeable host rock resulting in contact metamorphism. As fluids exsolve from the melt and leave the magma, metasomatism occurs. As the intrusion cools, meteoric fluids later infiltrate the system (Figure 2) (Einaudi et al., 1981; Meinert et al., 2005). Variables such as tectonic setting, magma composition, formation depth, and host rock compositions determine the skarn mineralogy and commodities (Figure 3) (Meinert et al., 2005). As heat and fluids propagate through the surrounding rocks, minerals such as garnet, pyroxene, epidote, and wollastonite, can form (Figure 4) (Einaudi et al., 1981; Meinert et al., 2005; Robb, 2005). Metal deposition can occur at various stages during skarn formation, with most deposition occurring during the final stage (Einaudi et al., 1981; Meinert et al., 2005; Robb, 2005).

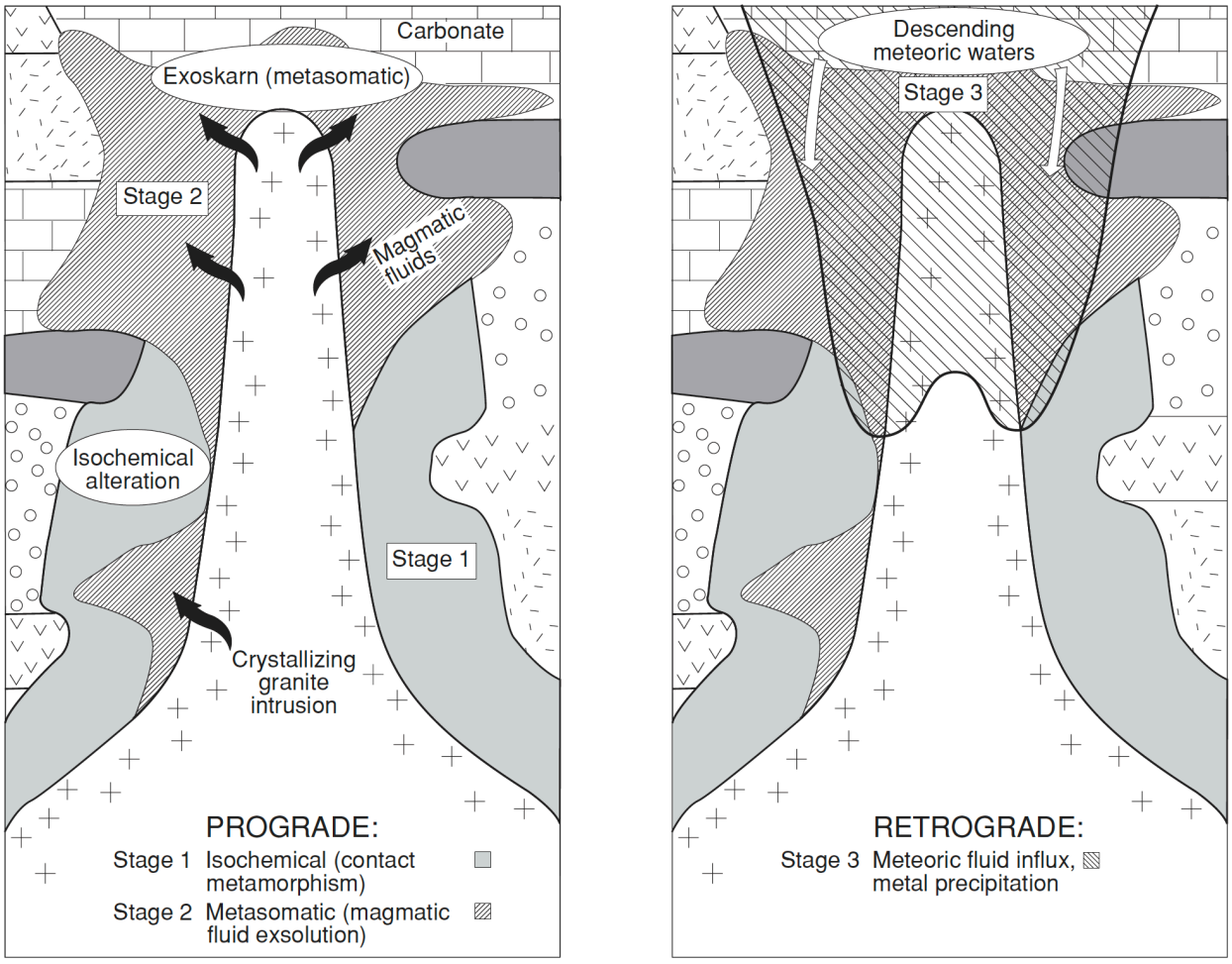

Figure 2. Simplified three-stage model of skarn formation associated with a magmatic intrusion from Robb (2005). The prograde stages occur during a local increase in temperature; the retrograde stage occurs as the system cools.

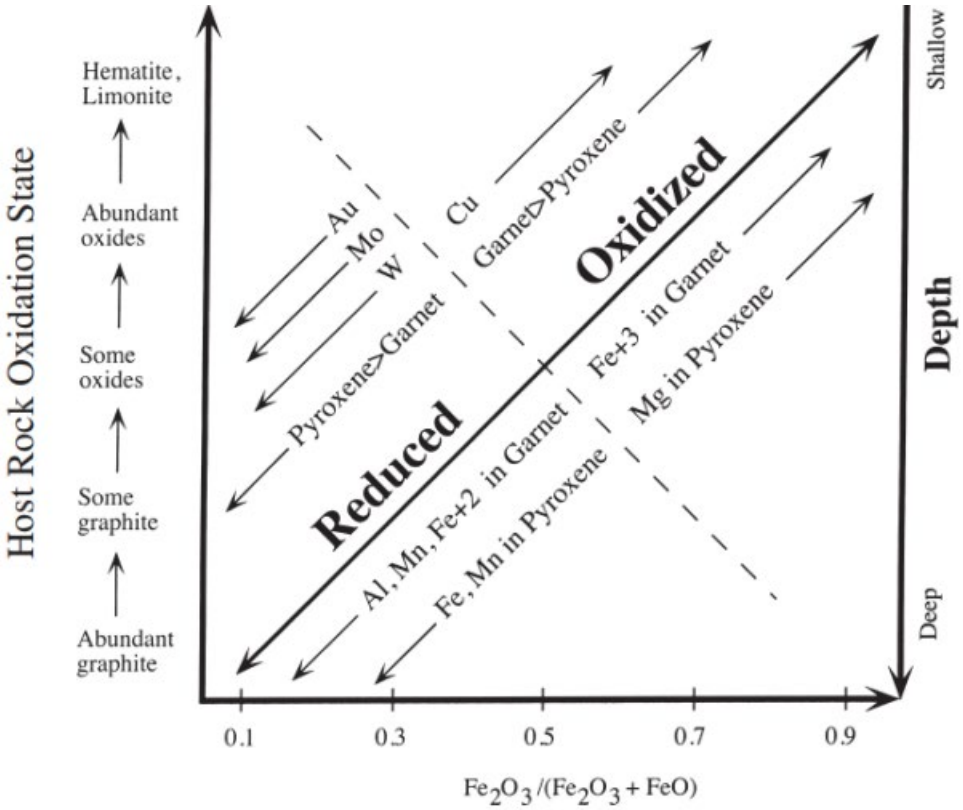

Figure 3. Schematic relationship of the oxidation state of the pluton and host rocks with commodity and mineral composition (Meinert et al., 2005).

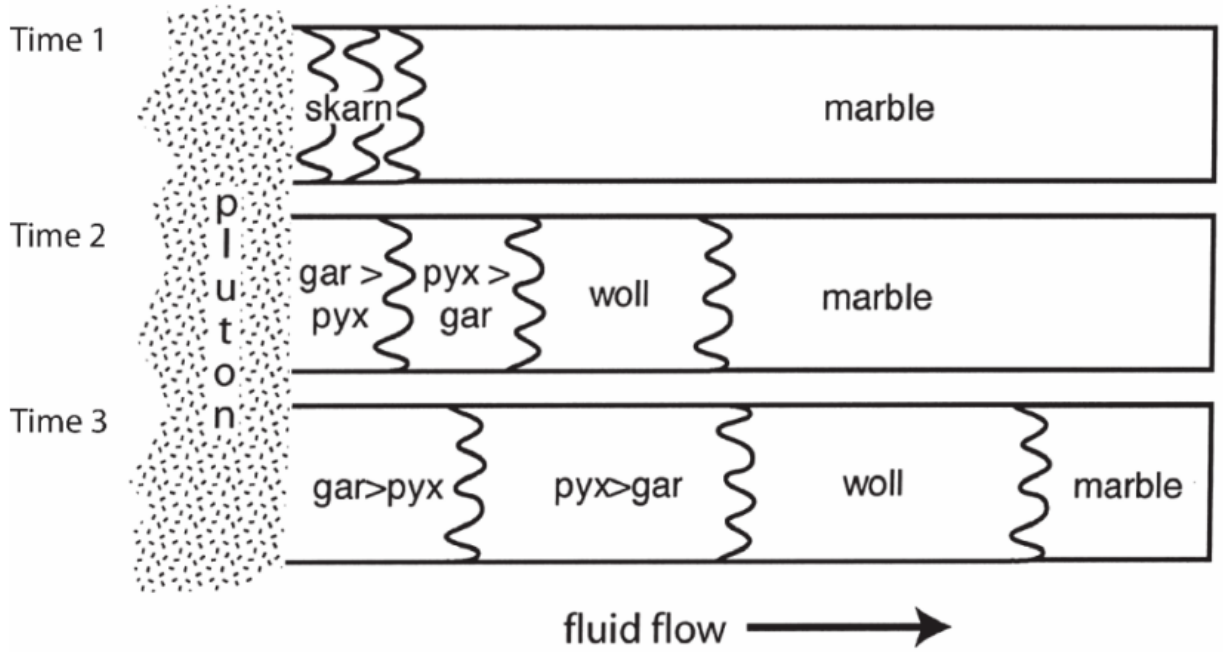

Figure 4. Sketch of reaction fronts resulting from episodic fluid flow during stages 1 and 2 of skarn formation (Meinert et al., 2005). Gar = garnet, pyx = pyroxene, woll = wollastonite.

2.3 The Fe skarns of Puerto Rico

Across the archipelago of Puerto Rico, there are many known metal deposits, including several that host Fe in Fe oxide minerals such as magnetite (Cox and Briggs, 1973). The target of this study is the Island Queen Fe skarn in eastern Puerto Rico, as it is a poorly studied but historically economic deposit (Figure 5) (Knoerr, 1952). This work complements a larger scale research effort between Auburn University and the University of Puerto Rico, Mayagüez to characterize and compare three Fe skarns in Puerto Rico: Island Queen, Keystone, and Tibes (Figure 5).

Skarns with Fe as a commodity ("Fe skarns") are only formed in island arc settings (Einaudi et al., 1981; Meinert et al., 2005). Most global Fe skarns that have been studied formed in island arc settings that had been accreted onto land post-deposition (e.g. the Xinqiao skarn, Wang et al., 2011; the Han-Xing skarn, Zhu et al., 2020). Due to Puerto Rico being an extinct island arc that has not been accreted, Island Queen, Keystone, and Tibes remain as they were originally deposited. This makes the island of Puerto Rico an exceptional natural laboratory to understand Fe transport and deposition in skarn systems.

2.3.1. Study site: the Island Queen skarn

The Island Queen skarn is located in the Humacao Quadrangle within the Pitahaya Formation in the CIP (M'Gonigle, 1978). This approximately 2000-meter-thick formation consists of interbedded lava, breccia, and tuff, and beds of limestone can be found up to 1-meter-thick throughout the formation (M'Gonigle, 1978). In some areas, lenses of pure magnetite have replaced the limestone beds, resulting in the formation of the Island Queen skarn (M'Gonigle, 1978).

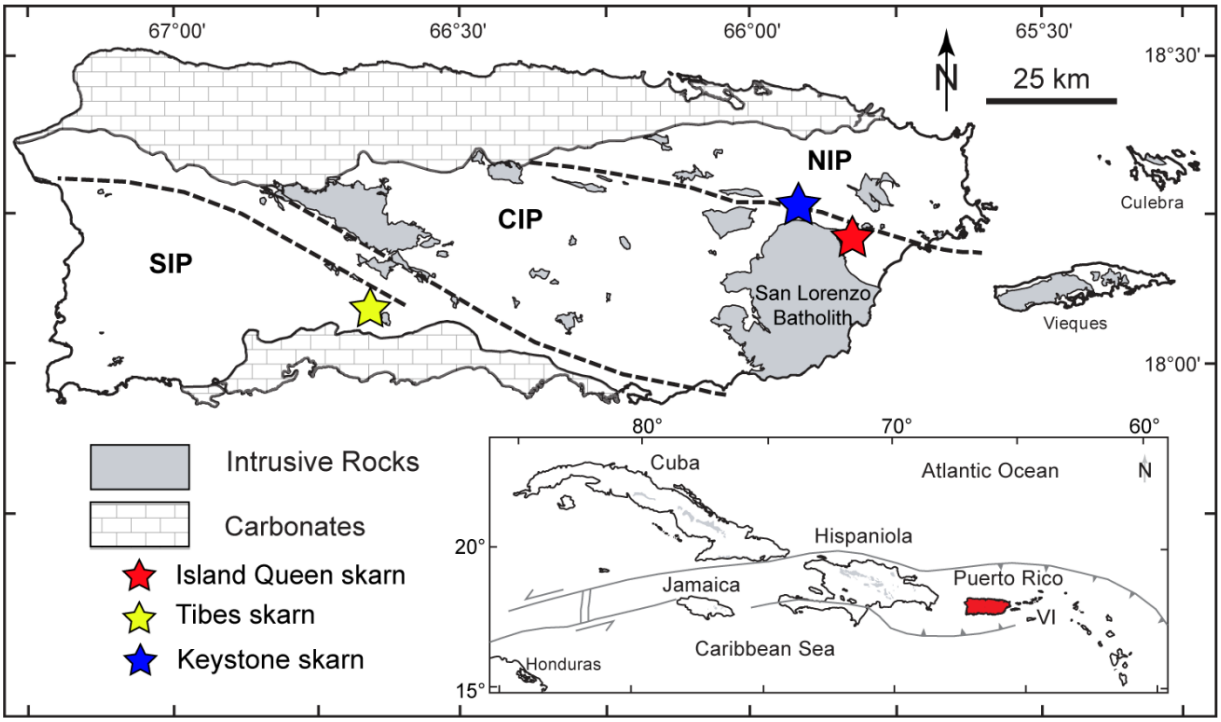

Figure 5. Simplified geologic map of Puerto Rico highlighting the geologic provinces (SIP, CIP, and NIP) separated by major fault zones (dashed lines), and the locations of three known iron skarns. White areas on the island represent complex local geology that has been omitted for clarity so that only information relative to this project is shown. See Appendix A for a more detailed geologic map. Base map by Dr. Thomas Hudgins, modified from Schellekens (1998).

3. Methods

3.1. Sample collection

A total of 18 samples were collected from the Island Queen skarn including magnetite ore and host rock samples with varying degrees of alteration (Table 1). Fourteen samples were collected from previous work done by collaborators at UPRM. Samples were collected from two areas within the Pitahaya Formation: one magnetite has replaced limestone (limestone lens) and another where ore exists as a massive magnetite body (MMB) (Figure 6). Due to vegetation growth and neighborhood developments, most of the ore body is not accessible for *in situ* sampling. However, historic mining and the neighborhood construction has made float available.

Table 1. List of Island Queen (IQ) samples. Mgt = magnetite, MMB = Massive Magnetite Body. UPRM = University of Puerto Rico, Mayagüez.

Sample	Description	Area	*In situ*/Float	Collected by
IQ-01	Mgt Ore	MMB	Float	UPRM
IQ-02	Mgt Ore	MMB	Float	UPRM
IQ-03	Mgt Ore	MMB	Float	UPRM
IQ-04	Mgt Ore	MMB	Float	UPRM
IQ-05	Mgt Ore	MMB	Float	UPRM
IQ-08	Mgt Ore	MMB	Float	UPRM
IQ-09	Mgt Ore	MMB	Float	UPRM
IQ-10	Mgt Ore	Lens	*In situ*	UPRM
IQ-11	Host Rock: Limestone	Lens	*In situ*	UPRM
IQ-12a	Host Rock: Limestone	Lens	*In situ*	UPRM
IQ-12b	Host Rock: Limestone	Lens	*In situ*	UPRM
IQ-13	Host Rock: Limestone	Lens	*In situ*	UPRM
IQ-14	Host Rock: Limestone	Lens	*In situ*	UPRM
IQ-15	Mgt Ore	MMB	Float	UPRM
IQ-16	Host Rock: Volcaniclastic	Lens	Float	This study
IQ-17	Host Rock: Volcaniclastic	Lens	Float	This study
IQ-18	Host Rock: Volcaniclastic	Lens	Float	This study
IQ-19	Host Rock: Volcaniclastic	Lens	Float	This study

3.2. Petrography

Hand specimen and thin section observations were used to identify ore, alteration, and secondary minerals and to assess the textures and relationships between individual minerals. Thin sections were analyzed using a Nikon Eclipse Ci POL petrographic microscope paired with a DS-Ri2 camera and NIS-Elements BR imaging software at Auburn University. Transmitted light was used for the transparent minerals (i.e. garnet, quartz, etc.) and reflected light was used for the opaque minerals (i.e. magnetite, hematite, and goethite).

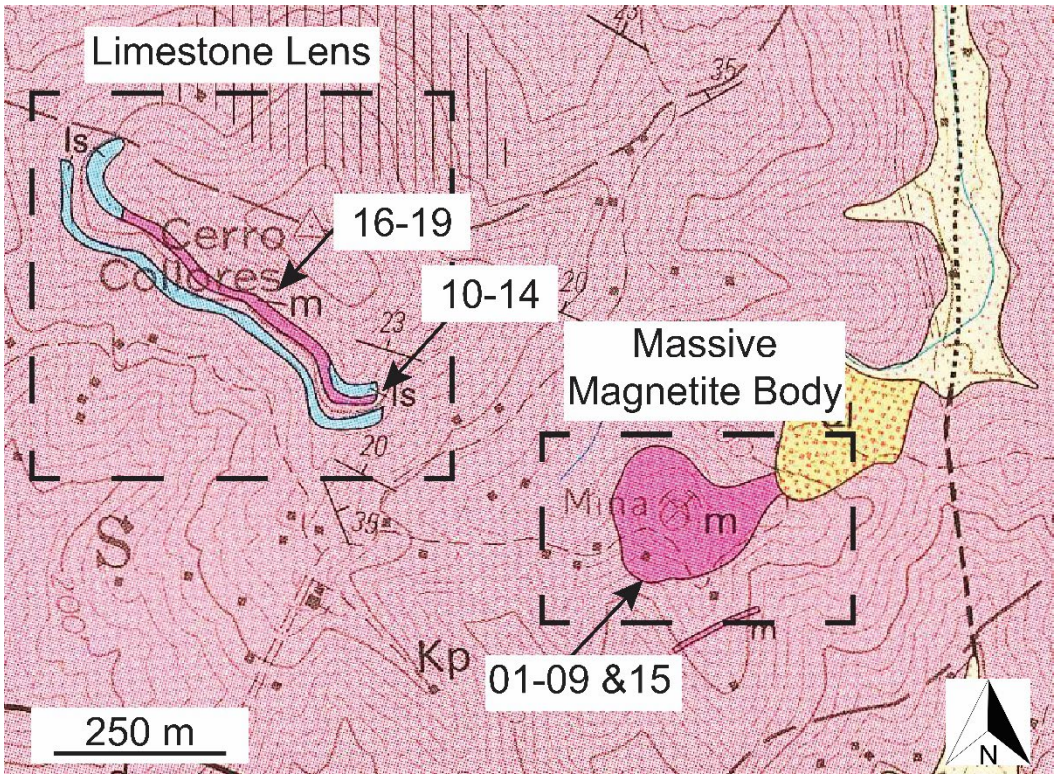

Figure 6. USGS Humacao Quadrangle map (M'Gonigle, 1978) with Island Queen sample locations. Areas of sample locations are indicated with dashed box, MMB = massive magnetite body, Lens = limestone lens. Light pink unit (Kp on map) is the Pitahaya Formation which is characterized as interbedded lava, breccia, and tuff. The light blue unit is the limestone (ls) lenses within the Pitahaya Formation that are replaced by magnetite (m, dark pink on map). Contour lines are at 20m intervals. Ql = landslide deposits, light yellow unit = alluvium deposits, Mina = old mine site, and square dots = location of houses. Strike and dip data are from M'Gonigle (1978).

3.3. Laser ablation inductively coupled mass spectrometry

In situ trace element concentrations were measured in Island Queen magnetite ore following Nadoll et al. (2014) and Dare et al. (2014) using laser ablation inductively coupled mass spectrometry (LA-ICP-MS). The analyses were performed with a 193nm Excimer laser (NWR193 by Elemental Scientific Lasers) attached to an Agilent 7900 ICP-MS. Prior to analysis, thin section maps were made of the magnetite ore samples using a Nikon Supercool Scan 5000. To account for instrumental drift and allow for quantitative data processing, analyses were also performed on standards NIST 610 and 612 from the National Institute of Standards and

Technology as well as the Columbia River Basalt Reference Material (BCR-2GA) from the United States Geological Survey.

Five to eight spots with a diameter of 30μm were chosen across each thin section, with care taken to avoid magnetite with visible alteration or holes. To avoid hitting the glass slide, spots were analyzed at a dwell time of 20 seconds at a frequency of 8Hz at 25% energy. Abundances of ^{23}Na, ^{24}Mg, ^{25}Mg, ^{27}Al, ^{29}Si, ^{43}Ca, ^{44}Ca, ^{47}Ti, ^{51}V, ^{52}Cr, ^{55}Mn, ^{56}Fe, ^{57}Fe, ^{59}Co, ^{60}Ni, ^{63}Cu, ^{66}Zn, ^{71}Ga, and ^{118}Sn were measured in each magnetite sample. The data were processed using the software iolite v.4 (Elemental Scientific Lasers). Iron mass 57 was used as the internal standard with concentrations of Fe measured with an Election Probe Microanalyzer (EPMA).

3.4. Electron probe microanalysis

EPMA work was done at Virginia Tech on a JEOL JXA-iHP200F that detects secondary electrons (SE) and backscattered electrons (BSE) and has an energy dispersive spectrometer (EDS) and five wavelength dispersive spectrometers (WDS). Elemental maps and WDS spot analyses were performed to quantify the abundance of Fe in magnetite and analyze the spatial distribution of key trace elements. To determine the elements of interest for WDS imaging, quick EDS scans and spot analyses were performed to understand the general composition of the sample. Areas with more than five elements present were mapped using EDS to analyze all elements present, and samples with subtle zonation were targeted for Fe and four trace elements of interest (e.g. Si, Ca, Mg, Ti, Al, Mn) to allow for higher resolution results. Elemental maps were acquired with beam conditions set to 20kV and 200nA with a dwell time of 100μs. Pixel size for mapping was adjusted accordingly to have a final run time of approximately five hours. Spot analyses using WDS were performed close to each LA-ICP-MS spot, avoiding any effects from the LA as well as alteration or holes present in the magnetite. Samples were analyzed by

standardizing with the magnetite standard 114887 from the National Museum of Natural History at the beginning and end of each session. Beam conditions were successful at 15kV and 20nA for spot analyses.

3.5. Iron isotope analysis

Nine magnetite, four volcaniclastic, and five limestone samples were prepared and measured for their stable Fe isotope compositions in the Pacific Centre for Isotopic and Geochemical Research (PCIGR) at the University of British Columbia (UBC) following the procedures of Bilenker et al. (2018) and King-Doonan et al. (2024). PCIGR is equipped with a class 1000 clean laboratory facilities with class 100 fume hoods for all geochemical preparation.

The magnetite ore samples were crushed, and impurities and visibly altered grains were removed by using non-magnetic tweezers. A hand-held magnet was used to separate approximately 2mg of pure magnetite for Fe isotope analysis. The host rock samples were also powdered; approximately 150mg of bulk rock powder was used for volcaniclastic samples and approximately 12mg for limestones. To prepare for Fe separation, all samples were dissolved fully in capped, cleaned Savillex vials on a hot plate at 120-130°C. Volcaniclastic samples were first dissolved in ultrapure concentrated HF and HNO_3, dried down, and then digested in concentrated HCl before being dried again. All powdered magnetite samples were fully dissolved in 4-8mL of aqua regia ($1HNO_3$:3HCl) and dried down.

In preparation for column chromatography following the procedures of Bilenker et al. (2018), all samples were redigested in 1mL 7N HCl and left on a hotplate at 120°C for a minimum of one hour. In clean BioRad columns, 1mL of BioRad AG MP-1M resin (100-200 mesh) was loaded, and conditioned with 10mL of 7N HCl. Once conditioned, the samples were loaded into the columns and rinsed with 7N HCl to remove matrix elements; the rinse for magnetite samples was 20mL and the rinse for whole rock samples was 40mL. To elute the Fe,

columns were then rinsed with 8mL of a 1N HF/0.5N HNO_3 solution into clean Savillex vials. The Fe solution was then left on the hot plate to dry. Finally, the samples were twice shot with concentrated HNO_3 and dried down before being redigested into 10mL of a 2% HNO_3 for analyses.

The Nu Plasma 1700 Multi-Collector Inductively Coupled Mass Spectrometer (MC-ICP-MS) was used to measure Fe isotope ratios with a DSN-100 desolating nebulizer. The Nu 1700 was run in dry plasma and high-resolution mode to fully resolve isobaric interferences on the ^{54}Fe, ^{56}Fe, and ^{57}Fe signals. For analysis, the USGS BCR-2 (Columbia River Basalt) was used as a reference material, and synthetic IRMM-14 metal from the Institute for Reference Materials and measurements was used as a standard for Fe. Concentrations of Fe were matched to within 10% between the reference materials and samples and the bracketing standard (IRMM-14) prior to analysis (King-Doonan et al., 2024). The MC-ICP-MS software corrected for the interference between ^{54}Fe and ^{54}Cr by monitoring ^{52}Cr and subtracting the ^{54}Cr. Standard-sample bracketing was used during analyses such that IRMM-14 was analyzed before and after every sample and reference material. Reference materials were analyzed throughout the runs to check for accuracy. Each sample was analyzed two to four times and results were reported in delta (δ) notation, relative to IRMM-14 using the equation:

$$\delta^{56}Fe = [(^{56}Fe/^{54}Fe)_{sample} /(^{56}Fe/^{54}Fe)_{IRMM\text{-}14})\text{-}1]*1000.$$

3.6. Oxygen isotope analysis

Bulk magnetite O isotope data were obtained by first crushing magnetite samples into a powder and sending ~2mg of the purest samples to the Stable Isotope Laboratory of Dr. Ilya Bindeman at the University of Oregon. Samples were using a MAT 253 gas isotope ratio mass spectrometer attached to a laser fluorination system (e.g. Bilenker et al., 2016). Due to the unavoidable presence of secondary minerals like goethite and limonite, samples were pre-treated

overnight to burn off materials that were not magnetite. These results are also reported in δ notation relative to Vienna-Standard Mean Ocean Water (V-SMOW) using the equation:

$$\delta^{18}O = [(^{18}O/^{16}O)_{sample} / (^{18}O/^{16}O)_{V\text{-}SMOW})\text{-}1]*1000.$$

6. Results

6.1. Field observations

Outcrop of the Island Queen magnetite ore is no longer reliably accessible in the field. Since the mining ban, previously mined areas have been developed into neighborhoods, and tropical vegetation growth is quick and unpredictable (Figure 7). However, there is some access to the volcaniclastics of the Pitahaya Formation. Recent aeromagnetic data generated by the USGS Earth MRI program will be a useful tool in locating or mapping other Fe deposits, but it will be crucial to ground-truth the data for accurate interpretations of whether Fe ore is present. At Island Queen, this is particularly important given that the volcaniclastic rocks that are accessible are weakly magnetic and their weathered products can appear to be magnetite. Despite a lack of access to outcrops of Island Queen, petrographic and geochemical analyses of the ore and host rocks can provide valuable information.

Figure 7. Island Queen skarn outcrop photos from the limestone lens area. Photos are taken in the same location two years apart showing rapid vegetation growth in the area completely covering the outcrop.

6.2. Petrography of the Fe ore

The Fe ore at Island Queen is predominately magnetite, ranging from anhedral to euhedral crystals (Figure 8). Each sample contains various secondary Fe oxide phases such as hematite, martite, goethite, and limonite. Hematite is typically tabular to needle-like (Figure 8B), whereas martite is predominantly seen as alteration along grain boundaries and along magnetite crystal planes (Figures 8A, C, D, E, F). In some cases, martite can be seen in the center of magnetite grains with a sponge texture (Figures 8C, 8D). Dissolution-reprecipitation (DR) textures are seen in samples IQ-05, IQ-08, and IQ-15 (Figures 8E, 8F). Where DR textures are pervasive, like in sample IQ-15, there is an alignment of individual grains that appears to reflect directional growth (Figure 8E). Minor goethite is observed within the ore as well (Figures 8A, 8F), and limonite is present primarily as a weathering product; IQ-04 ore contains the highest proportion of limonite as an orange powder coating on magnetite grains. Accessory minerals in all ore samples include quartz and chlorite, with anhydrous garnets observed in samples IQ-01 and IQ-10.

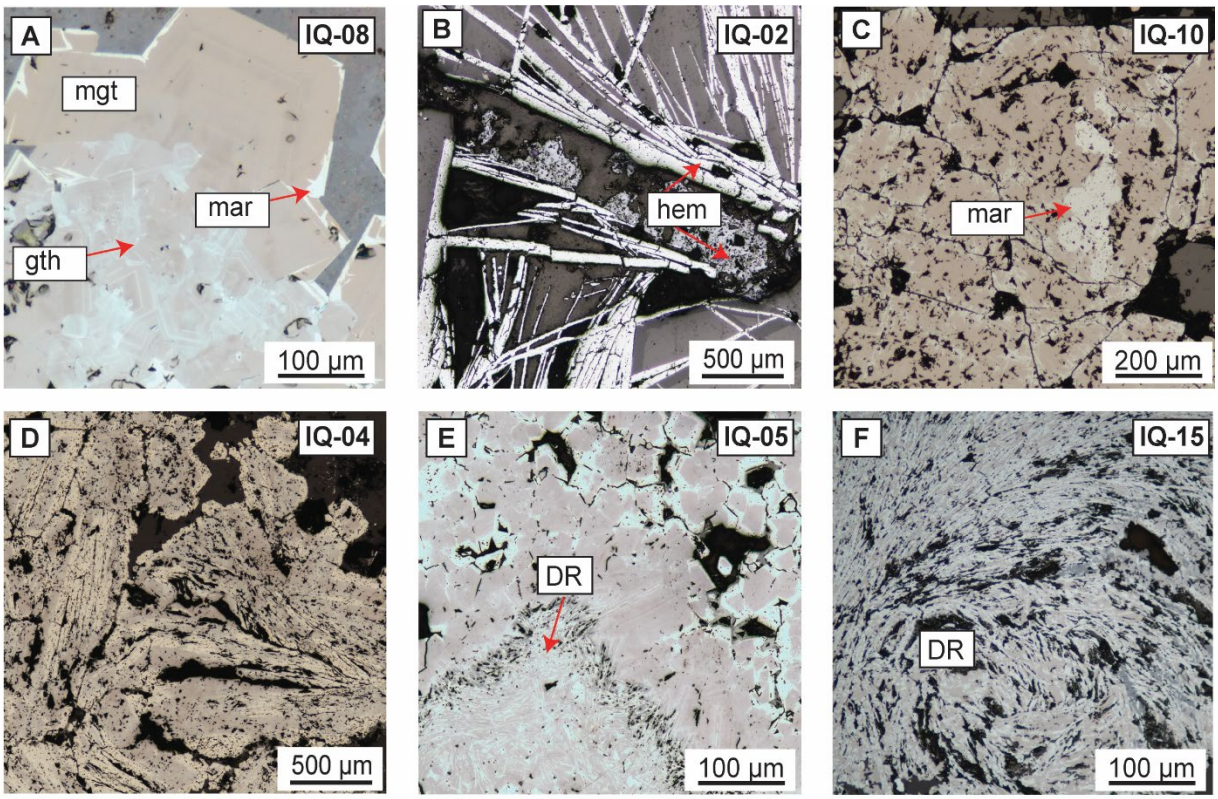

Figure 8. Representative reflected light photomicrographs of Island Queen ore samples. **(A)** Sample IQ-08: euhedral zoned magnetite (mgt) crystals with alteration into martite (mar) along grain boundaries and goethite (gth) at the center. Fine grain gray mineral surrounding magnetite is goethite. **(B)** Sample IQ-02: needle-like hematite (hem) and finer grained hematite surrounded by quartz. **(C)** Sample IQ-10; euhedral magnetite (brown) with sponge-like martite (mar) alteration in the center of the crystals. **(D)** Sample IQ-04: Tabular magnetite (brown) with sponge-like martinization (white) in the center of the crystals. **(E)** Sample IQ-05: magnetite (brown) crystals showing subtle zonation and alteration to martite (white) along the edges of the magnetite. The dissolution-reprecipitation (DR) texture is present in the sample, in this area there is a larger proportion of alteration to martite and goethite (gray). Black areas represent voids. **(F)** Sample IQ-15: dissolution-reprecipitation (DR) texture with a directional growth of magnetite (brown) with alteration to martite (white) and goethite (gray). Black areas represent voids.

6.3. Elemental composition of the Fe ore

The magnetite samples measured by EPMA have an average Fe content of 65.2wt% (Table 2, a full dataset is listed in Appendix B). Aside from some subtle zonation, the Fe content is mostly consistent across each thin section and throughout individual magnetite grains. There is a decrease in Fe concentration observed in EPMA element maps, but this is likely to reflect the

presence of goethite (Figure 8A). Trace element concentrations, measured by LA-ICP-MS, are heterogeneous throughout individual samples, and a full table of results for all the elements analyzed can be found in Appendix C. Elements that are present in significant concentrations include Mg, Al, Si, Ca, Ti, V, Cr, Mn, Co, and Ni (Table 3).

Table 2. Average Fe wt% values measured by EPMA of magnetite grains in the ore samples.

Sample	IQ-01	IQ-02	IQ-03	IQ-04	IQ-05	IQ-08	IQ-09	IQ-10	IQ-15
Fe wt%	66.4	65.3	64.4	64.2	63.6	65.5	64.5	67.5	65.0

Table 3. Average relevant trace element concentrations (ppm) of the magnetite grains measured by LA-ICP-MS.

Sample	^{24}Mg	^{27}Al	^{29}Si	^{44}Ca	^{47}Ti	^{51}V	^{52}Cr	^{55}Mn	^{59}Co	^{60}Ni
IQ-01	250.4	982.3	5744.3	944.6	552.1	136.2	19.8	2395.6	89.8	112.2
IQ-02	338.3	2056.2	14434.6	987.8	276.0	64.8	19.5	2005.5	168.1	2.6
IQ-03	1241.3	3506.1	15422.5	521.1	302.1	104.7	83.1	850.3	104.4	7.7
IQ-04	319.7	2824.3	14684.9	1943.1	1462.8	180.0	34.1	1556.9	64.0	9.3
IQ-05	509.4	2009.3	20421.9	1213.4	102.7	57.8	3.7	1447.5	63.3	6.3
IQ-08	225.8	1383.5	11478.3	1177.7	272.7	43.0	8.1	3102.4	89.2	5.2
IQ-09	1128.4	6431.5	15512.4	3497.4	16897.0	1009.5	147.0	1146.8	138.2	57.0
IQ-10	505.0	2428.4	1859.2	285.6	545.8	247.6	12.9	1763.4	76.5	251.8
IQ-15	1238.5	3768.4	13865.3	399.6	97.0	58.5	6.1	652.8	85.1	7.4

Most of the Island Queen magnetite ore samples are geochemically zoned. The zonation is observed in both reflected light microscopy (Figure 8A), BSE images, and elemental maps (Figure 9, Appendix D). Oscillatory zonation of Fe and trace amounts of Si is present in most samples (Figure 9). Minor zonation of other trace elements like Ca is present in most samples. The Fe content difference between magnetite, hematite, and martite is subtle in EPMA imaging,

so it is difficult to distinguish between the individual Fe oxides. DR reaction textures have a slight increase in Mg, Si, and Ca (Figure 10). One sample (IQ-09) has Ti-rich lamellae in magnetite grains, interpreted to be ilmenite exsolution (Figure 11); reflected light microscopy of IQ-03 revealed a similar texture in rare grains.

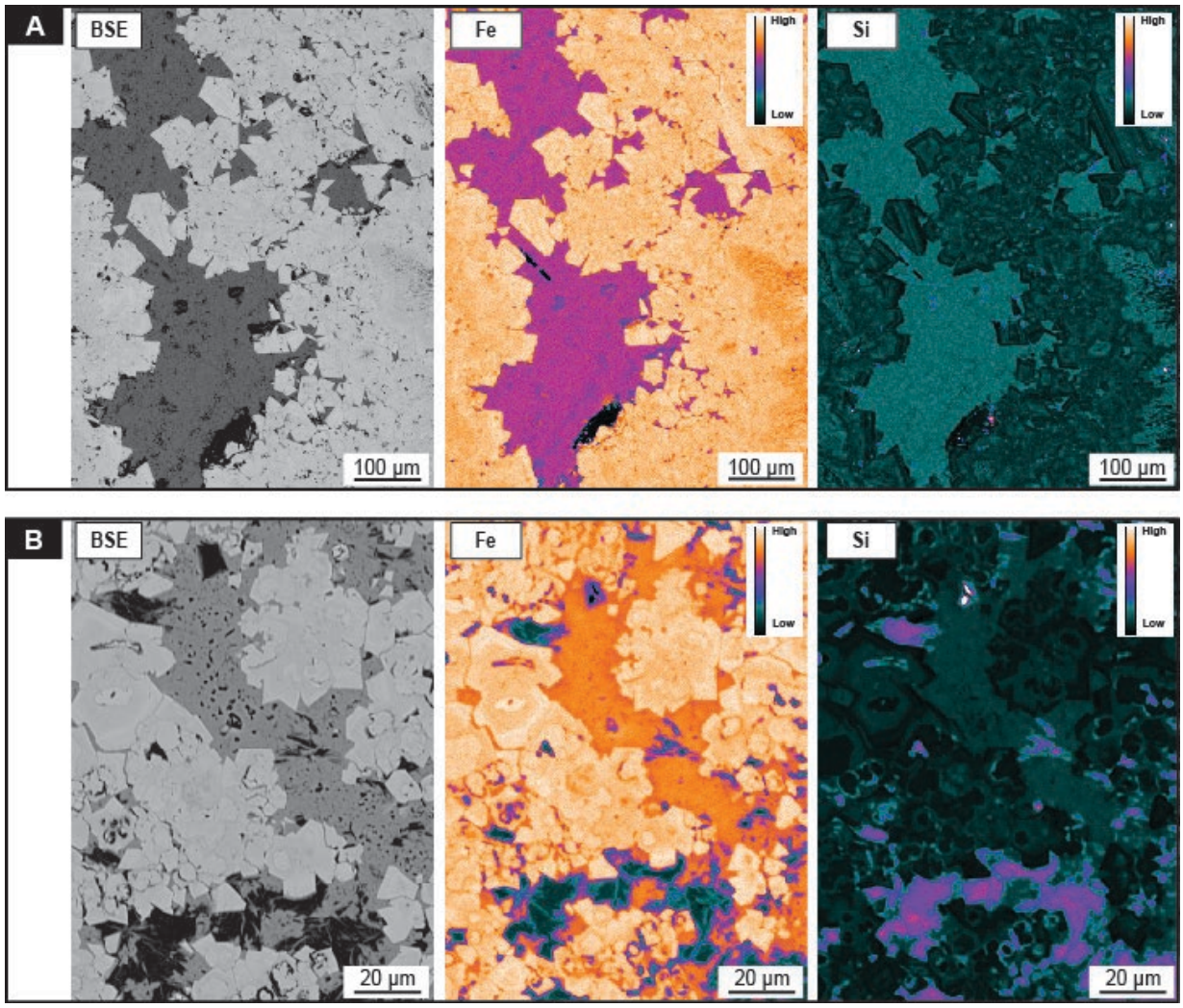

Figure 9. (A) BSE, Fe, and Si maps of IQ-08 magnetite (light gray in BSE) and goethite (dark gray BSE). Oscillatory zoning of Fe and Si is observed in magnetite grains, and a decrease in Fe concentration is observed between goethite and magnetite. **(B)** BSE, Fe, and Si maps of IQ-03 magnetite (light gray BSE) and hematite (dark gray BSE) with chlorite present (black BSE). Oscillatory zoning of Fe and Si is observed. Slight decrease in Fe concentration indicates magnetite versus hematite.

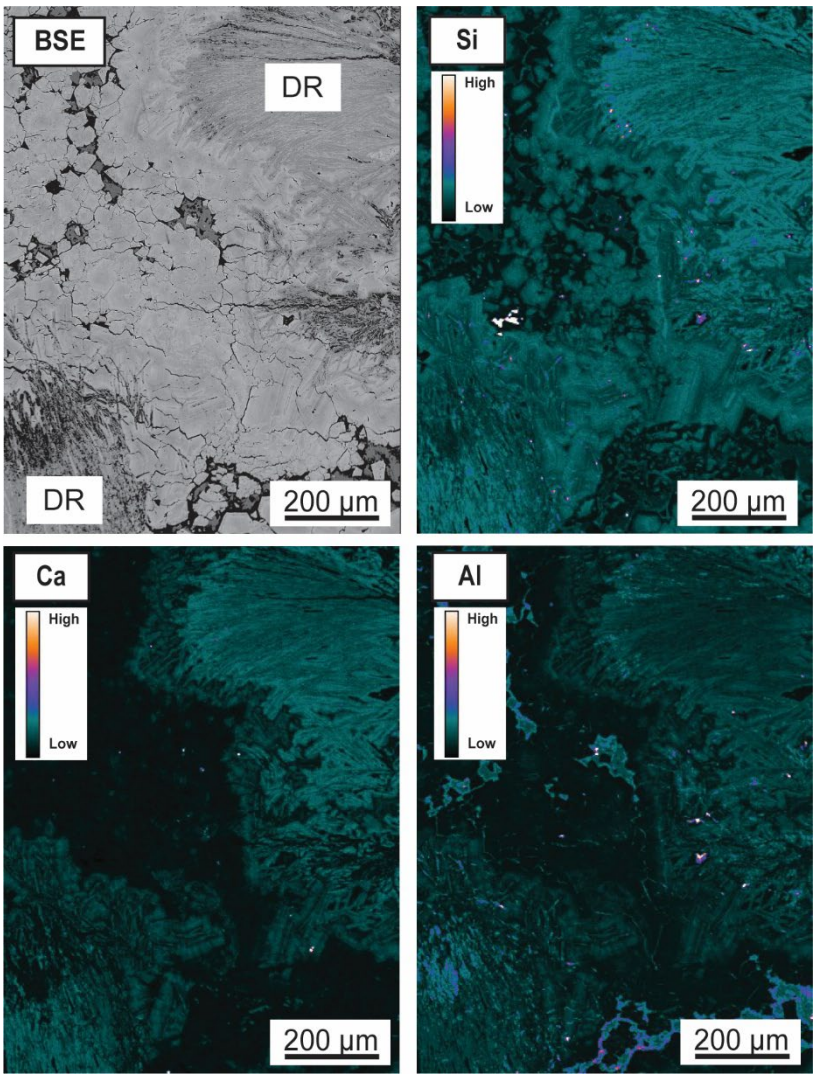

Figure 10. BSE, Si, Ca, and Al maps of IQ-05 magnetite with DR textures present. Reaction fronts show slightly increased concentrations of Si, Ca, and Al.

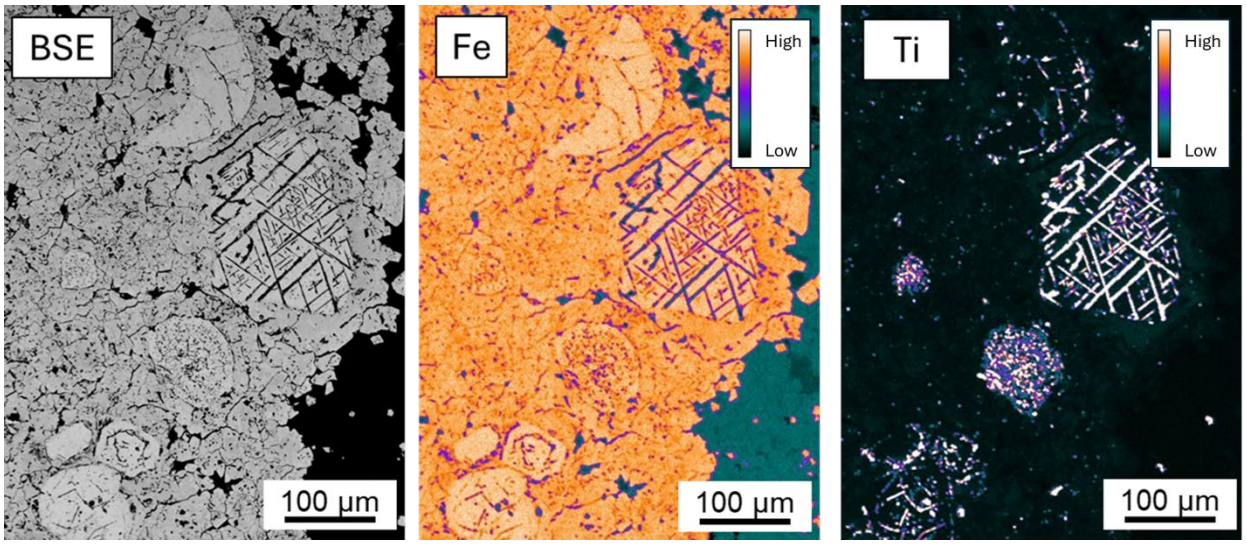

Figure 11. BSE, Fe, and Ti maps of IQ-09 magnetite (light grey in BSE) with ilmenite (bright white in Ti map) exsolution. The Ti map shows Ti-rich lamellae in magnetite.

6.4. Stable isotope compositions of Fe ore and host rocks

The Fe isotope compositions of nine Island Queen ore samples are heterogeneous and have a wide range in δ^{56}Fe values (±2σ, twice the standard deviation; n=number of analyses), from -0.41‰ ±0.05 to +0.28‰ ±0.07 (Table 4). The δ^{56}Fe values of seven of the magnetite samples range from -0.33‰ ±0.04 (n=3) to -0.02‰ ±0.01 (n=3). IQ-09 is an outlier; both duplicates have the heaviest δ^{56}Fe values: +0.11‰ ±0.04 (n=3) and +0.28‰ ±0.07 (n=2). IQ-08 had three duplicates measured with a large spread of δ^{56}Fe values: -0.12‰ ±0.06 (n=2), -0.22‰ ±0.04 (n=3) and -0.41‰ ±0.05 (n=2). Iron isotope compositions of the host rocks (limestone and volcaniclastics) are consistently isotopically heavier than the magnetite. The five limestones δ^{56}Fe values ranged from +0.11‰ ±0.05 to +0.30‰ ±0.05 and the four volcaniclastics ranged from +0.05‰ ±0.02 to +0.19‰ ±0.00. Preliminary O isotope ratios have been measured for four of the magnetite samples (Table 4). The δ^{18}O (±2σ) values range from -2.77‰ ±0.07 to +2.56‰ ±0.07.

Table 4. Average $\delta^{56}Fe$ and $\delta^{18}O$ values of Island Queen samples. Blank cells = samples that do not have corresponding $\delta^{18}O$ values, * = samples that had duplicates of Fe isotope run and results were averaged, n = number of analyses, σ = standard deviation.

Sample type	Sample	$\delta^{56}Fe$	±2σ	n	$\delta^{18}O$	±2σ
Magnetite	IQ-01	-0.33	0.04	3	+1.02	0.07
Magnetite	IQ-02	-0.27	0.03	3	-1.79	0.07
Magnetite	IQ-03*	-0.03*	0.03*	4*	+2.56	0.07
Magnetite	IQ-04	-0.02	0.01	3		
Magnetite	IQ-05	-0.17	0.05	5	-2.77	0.07
Magnetite	IQ-08	-0.22	0.04	2		
Magnetite	IQ-08 DUP	-0.41	0.05	3		
Magnetite	IQ-08 DUP2	-0.12	0.06	2		
Magnetite	IQ-09	+0.11	0.04	3		
Magnetite	IQ-09 DUP	+0.28	0.07	2		
Magnetite	IQ-10	-0.07	0.07	3		
Magnetite	IQ-15	-0.20	0.02	2		
Limestone	IQ-11	0.00	0.05	2		
Limestone	IQ-12a*	0.13*	0.06*	5*		
Limestone	IQ-12b	+0.17	0.03	2		
Limestone	IQ-13*	+0.23*	0.01*	4*		
Limestone	IQ-14	+0.30	0.05	2		
Volcaniclastics	IQ-16	+0.10	0.03	2		
Volcaniclastics	IQ-17	+0.19	0.00	3		
Volcaniclastics	IQ-18	+0.09	0.02	2		
Volcaniclastics	IQ-19	+0.05	0.03	2		

7. Discussion

7.1. Textural and trace element geochemistry evidence for fluid origin and alteration history

Magnetite textures can be used to determine ore fluid origin in conjunction with geochemistry. All the magnetite samples analyzed have secondary minerals such as martite, goethite, limonite, and hematite, indicating various degrees of alteration (Figure 8). The DR texture observed in some of the samples (e.g., Figures 8E, 8F) is evidence that later hydrothermal

fluids dissolved existing magnetite and reprecipitated oxide minerals such as martite (Hu et al., 2015; Yin et al., 2022; Hu et al., 2023). The volume change associated with replacing magnetite with martite produces the pattern and voids (e.g., Figures 8E, 8F) (Yin et al., 2022). The DR reaction fronts are enriched in elements such as Si, Ca, and Al (Figure 10), which were abundant in the Island Queen system where limestone lenses reacted with hydrothermal skarn fluids of magmatic or meteoric origin. This is consistent with observations in the literature of magnetite with DR textures containing higher concentrations of fluid mobile elements (Si, Ca, Al, and Mg) at the reaction fronts (Hu et al., 2015; Hu et al., 2023).

The composition and conditions of the geologic fluid(s) (silicate melt, hydrothermal, and/or meteoric) that formed the magnetite ore at Island Queen are reflected in its trace element geochemistry (Dupuis and Beaudoin, 2011; Dare et al., 2014; Nadoll et al., 2014; Bilenker et al., 2016). The trace element concentrations of key elements (Ti, V, Ca, Al, and Mn) measured using LA-ICP-MS are used to compare the Island Queen skarn magnetite samples to one another and to the compositions of global skarns and other ore deposit types (Figure 12). In general, higher concentrations of Ti+V indicate that the fluids responsible for magnetite formation were higher in temperature and most likely magmatic in origin (Dupuis and Beaudoin, 2011; Dare et al., 2014; Nadoll et al., 2014; Knipping et al., 2015). The variation in compositions within individual grains within the same sample reflect the evolution of the ore fluid during magnetite formation, growth, and alteration (Figure 12). The magmatic signature of the magnetite is preserved to varying extents in the trace element compositions of the Island Queen samples, but most strongly in IQ-04 and IQ-09 (Figure 12).

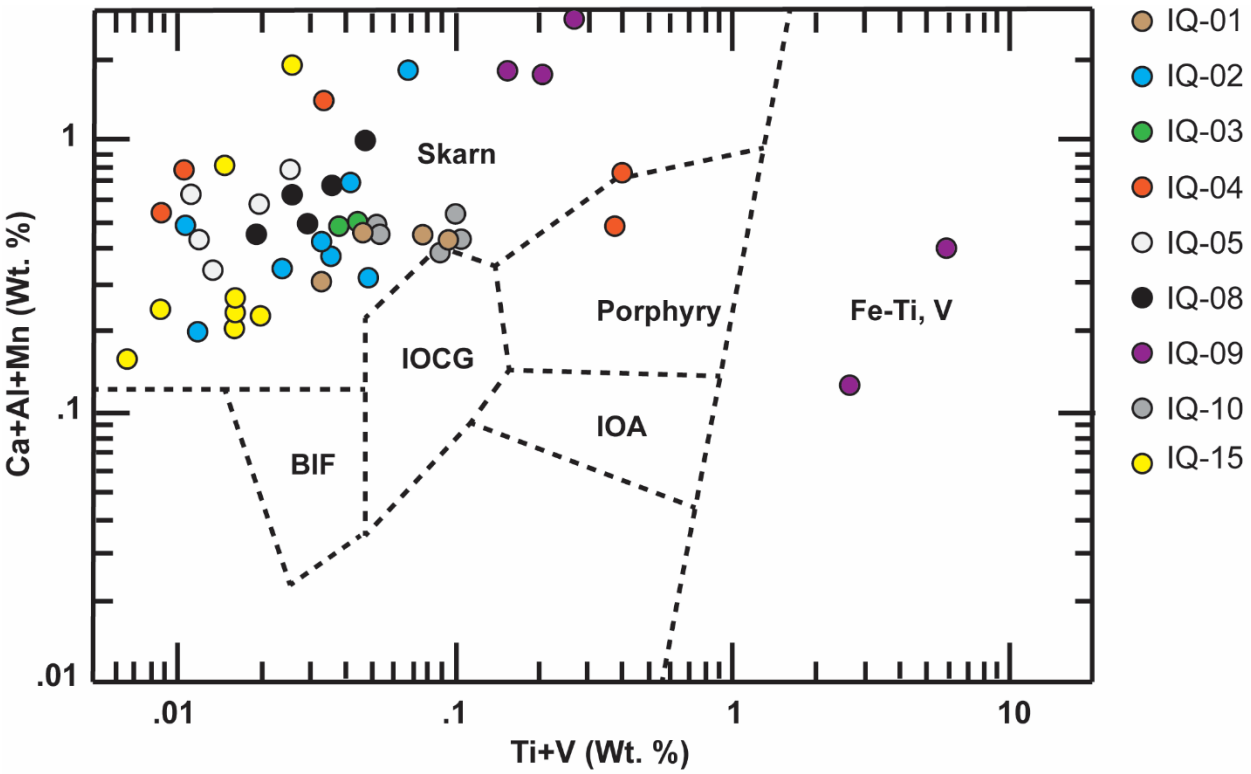

Figure 12. Plot of Ti+V (wt%) vs. Ca+Al+Mn (wt%) measured in the Island Queen magnetite. Values primarily plot within the skarn field, as expected. BIF = Banded Iron Formation; IOCG = Iron Oxide-Copper-Gold; IOA =Iron Oxide-Apatite (after Dupuis and Beaudoin, 2011).

Elemental compatibility and mobility can be used to interpret the observed compositional variations (Dare et al., 2014; Nadoll et al., 2014; Knipping et al., 2015; Hu et al., 2023). Generally, Ti and Al are considered fluid-immobile in a melt and are expected to be enriched in magnetite that crystallized from a magma while fluid-mobile elements such as, Si and Ca will be relatively less abundant (Dare et al., 2014). Hydrothermal magnetite is predicted to be enriched in Ni and V and depleted in Ti and Al compared to magmatic magnetite (Dare et al., 2014). The concentrations of these elements in the Island Queen magnetite primarily indicate a hydrothermal fluid signature except for two samples: IQ-03 and IQ-09 (Figure 13). Sample IQ-09 contains ilmenite exsolution (Figure 11) and a lack of Si zoning in magnetite grains, which indicates that it did not experience a significant amount of hydrothermal fluid overprinting and preserved a magmatic signature (Tan et al., 2016). The Ti, Ni, and Cr composition of IQ-03 also supports the

interpretation of a magmatic signature, which is controlled by the low Ni concentration of this magnetite (Figure 13). Furthermore, ilmenite exsolution was observed in IQ-03 as IQ-09 (Figure 11), and IQ-03 contained trace rutile. However, the Ti and V concentrations of IQ-03 are consistent with a hydrothermal signature (Figure 14). This indicates that IQ-03 partially preserved its primary magmatic composition but experienced more lower temperature alteration than IQ-09, which has Ti and V concentrations consistent with a magmatic origin.

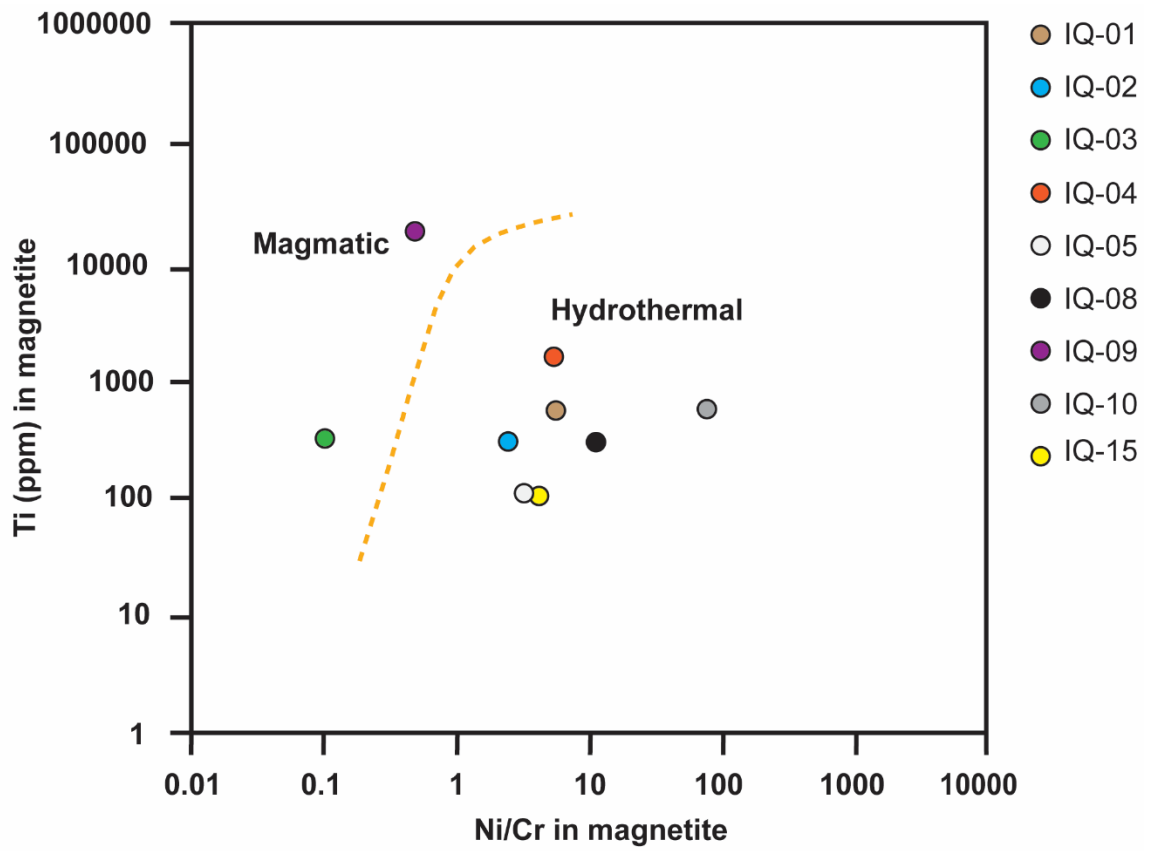

Figure 13. Plot of Ni/Cr vs. Ti (ppm) measured in the Island Queen magnetite. There are two outliers: IQ-09 has high Ti concentrations and IQ-03 has low concentrations of Ni, shifting the points into the magmatic range (after Dare et al., 2014).

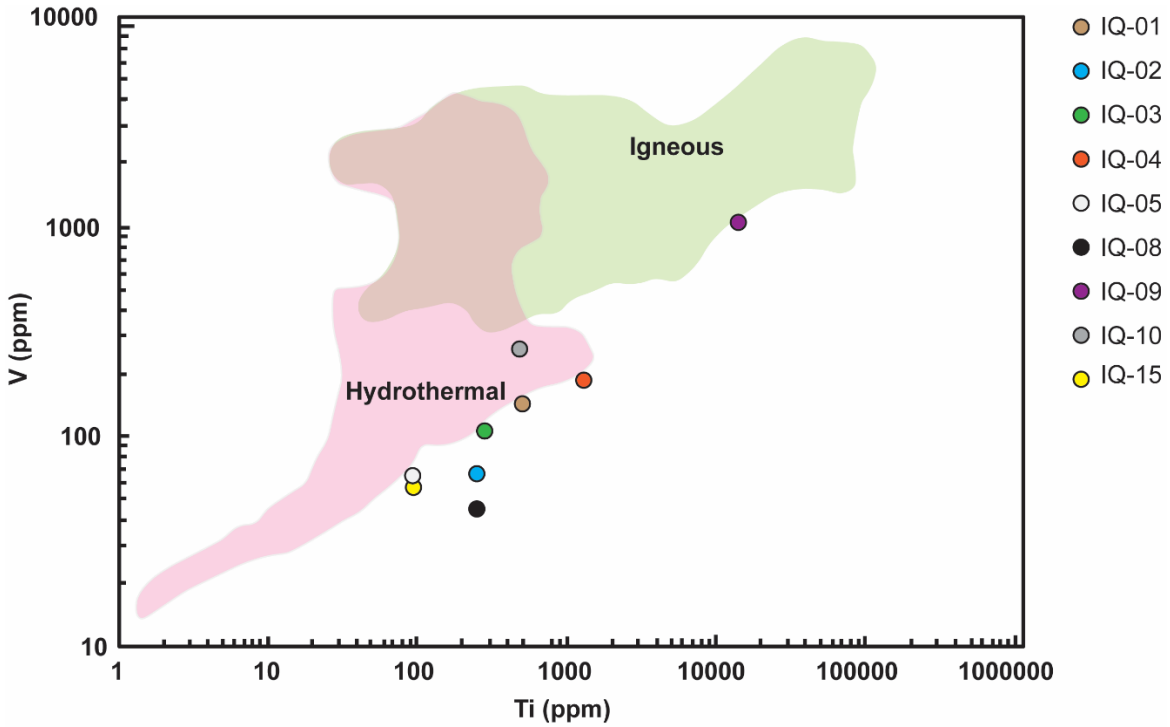

Figure 14. Plot of Ti (ppm) vs. V (ppm) of Island Queen magnetite. All samples, except IQ-09, are consistent with the hydrothermal field, which is based on a limited selection of global samples. The high concentrations of V and Ti in IQ-09 magnetite makes it more consistent with an igneous signature, supported by microscopic observations of ilmenite exsolution (after Knipping et al., 2015 and Hu et al., 2023).

7.2. Stable isotope composition as evidence for magnetite fluid source

Stable Fe and O isotope ratios measured in magnetite ore have been used to further refine the fluid origin in Fe oxide deposits (Bilenker et al., 2016; Simon et al., 2018; Troll et al., 2019). The method of pairing Fe and O isotopes in magnetite is based on the methods of Hedenquist and Lowenstern (1994), who used stable O and H isotopes to identify ore fluid source in fluid inclusions of epithermal deposits. Generally, magnetite with lighter Fe or O isotopic compositions indicates a lower temperature fluid origin, typically meteoric. Alternatively, magnetite from a higher temperature, magmatic origin is expected to have a heavier isotopic signature (Bilenker et al., 2016). The Fe and O isotope pairs available so far for the Island Queen skarn are shown in Figure 15. These values are consistent with a lower temperature fluid signature, consistent with alteration or non-magmatic fluids (Simon et al., 2018). Additional O

isotope data are needed to further constrain the fluid origin of the Island Queen ore, but this preliminary interpretation is consistent with petrographic observations and trace element datasets.

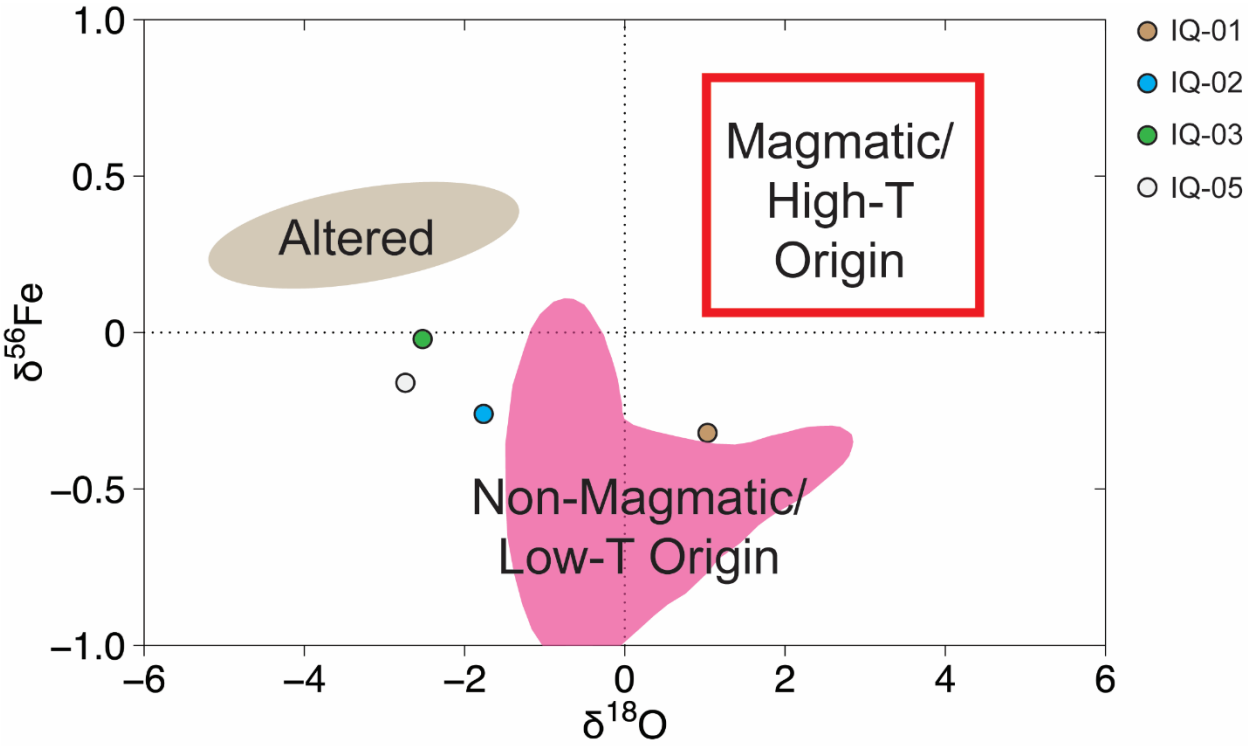

Figure 15. General diagram of $\delta^{56}Fe$ vs. $\delta^{18}O$ values of Island Queen magnetite where 0‰ represents the synthetic standard IRMM-14 and SMOW, respectively. The fields for Altered, Non-magmatic/Low-Temperature (T), and Magmatic/High-T magnetite are based on global compilations of magnetite from a variety of ore deposits (after Simon et al., 2018). (Magmatic ranges after Taylor, 1968; Bindeman, 2008; Heimann et al., 2008; Bilenker et al., 2016.)

The typical magmatic range of magnetite $\delta^{56}Fe$ values varies between 0.06‰ and 0.86‰ (Heimann et al., 2008; Bilenker et al., 2016). The Fe isotope signatures of Island Queen magnetite are most consistent with lower temperature, non-magmatic fluids except for IQ-09, which has a heavier isotopic signature (Figure 16). Importantly, petrography and EPMA results show that martite and hematite exist on a microscopic scale, such that the powders used for

isotopic analyses unavoidably contained unknown proportions of Fe oxides that were not primary magnetite. Regardless, the wide range in the magnetite Fe isotope values are consistent with variations in the trace element concentrations and supports later meteoric fluid overprinting of magmatic magnetite at various degrees.

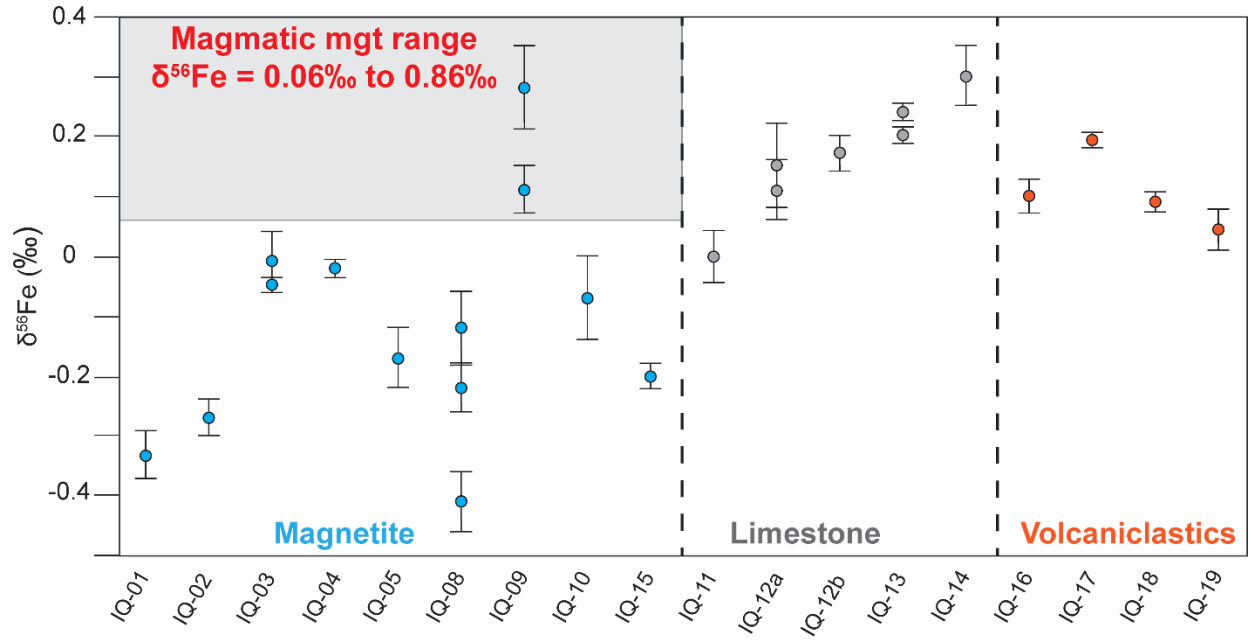

Figure 16. Plot of δ^{56}Fe values of Island Queen magnetite (mgt) and bulk rock limestone and volcaniclastics. (Magnetite magmatic range after Heimann et al., 2008; Bilenker et al., 2016.)

7.3. Fluid-rock reactions preserved in the Fe isotope ratios of Island Queen host rocks

The Fe isotope values for the host rock limestones and volcaniclastics are higher and have less variation between samples (Figure 16). It is important to note that all host rock samples contain variable proportions of magnetite that may be reflected in the δ^{56}Fe values. For instance, the *in situ* magnetite sample (IQ-10) represents an almost complete replacement of the limestone host rock. This sample has a lower δ^{56}Fe value than the limestones. This implies that the processes resulted in the magnetite replacement involved meteoric fluids, or a fluid that preferentially transported isotopically light Fe (e.g., reduced or chlorine-rich). The bulk rock

sample IQ-12a is mainly composed of limestone, and IQ-12b is a magnetite vein located within IQ-12a. IQ-13 is a magnetite-rich vein within another section of the same limestone lens. The limestone samples with more magnetite have higher δ^{56}Fe values, which suggests that the magnetite in these samples formed from a higher temperature fluid, potentially earlier in the formation of the skarn. As later, cooler, possibly meteoric fluids infiltrated the system, additional Fe was mobilized and limestone replaced. Additional O isotope data would provide more insight into the proportions of different fluids that contributed to forming the Island Queen skarn.

7.4. Comparison with other Puerto Rican skarns and global Fe skarns

The three skarns in Puerto Rico that have been studied using field, petrographic, and geochemical analysis include Island Queen: this study; Tibes: Barefoot, 2021 and Giovannetti-Nazario; Keystone: Patrick, 2023. The similarities and differences preserved in the ore are summarized in Table 5. Magnetite ore from the Tibes skarn has a magmatic signature (Barefoot, 2021) while Keystone and Island Queen magnetite is associated with a lower temperature hydrothermal origin (Patrick, 2023). The ~16 Tibes magnetite ore bodies are located close to the small igneous stock, resulting in a shorter-lived system and minimal, if any, meteoric input (Barefoot, 2021; Giovannetti-Nazario, 2022). Keystone and Island Queen are both associated with the San Lorenzo batholith and the magnetite ore bodies are found farther away from the intrusion (Patrick, 2023). DR textures along with trace element and stable Fe and O isotope data indicate that Keystone and Island Queen experienced a greater amount of late-stage meteoric water input. Magnetite from all three skarns have oscillatory zoning of Fe and Si in the magnetite (Barefoot, 2021; Patrick, 2023). Both Tibes and Keystone magnetite ore samples have pyrite present in the samples while Island Queen does not; all three locations have garnet present, although the Tibes garnet is much coarser and abundant (Barefoot, 2021; Patrick, 2023). Island Queen and Keystone have similar martite alteration (DR textures) while the Tibes magnetite

lacks abundant secondary Fe oxide phases. Tibes does contain, however, zonation of Si-rich micro inclusions (Barefoot, 2021).

Table 5. Summary table comparing key characteristics of the three Puerto Rican skarns.

Characteristic	Island Queen	Keystone	Tibes
Host Rock	Limestone	Volcaniclastics	Limestone
Pluton	San Lorenzo Batholith	San Lorenzo Batholith	Diorite stock
Fe-Si zoning in magnetite?	✓	✓	✓
Garnets present?	✓ (Small)	✓ (Small)	✓ (Large)
Si inclusions in magnetite?	X	✓	✓
Dominate ore fluid source	Meteoric	Meteoric	Magmatic
Field accessibility	Not accessible	Accessible on private property	Accessible

Island Queen has the lightest overall Fe isotope composition of the three deposits, and the largest variation across the dataset (Figure 17). This is likely evidence of more abundant later stage meteoric fluids interacting with the ore to varied extents. The preliminary O isotope values available for Island Queen match the Fe isotope trends in that the values are isotopically lighter than Keystone and Tibes and have a larger range (Figure 18). Overall, the Fe and O stable isotope compositions of the magnetite of all three skarns are consistent with skarns analyzed globally (Figures 17 & 18) (Fe isotopes: Wang et al., 2011; Zhu et al., 2020; O isotopes: Troll et al., 2019, Oyman, 2010, Dong et al., 2021, Xie et al., 2017).

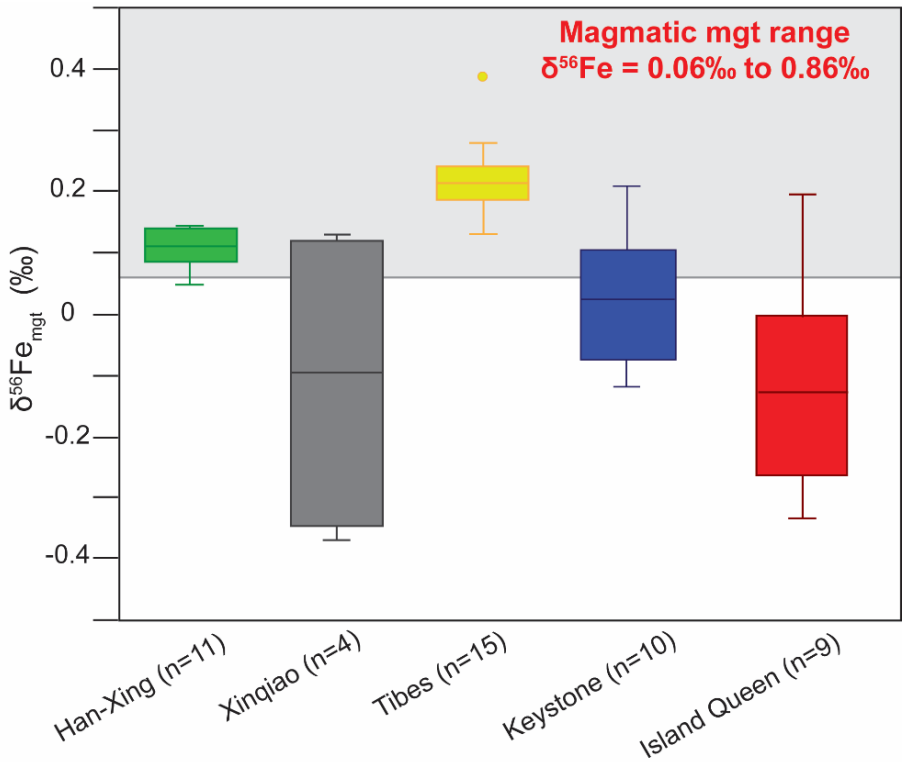

Figure 17. Iron isotope plot of the magnetite (mgt) from the three studied Fe skarns in Puerto Rico (Tibes, Keystone, Island Queen) compared to the two other Fe skarns with published $\delta^{56}Fe$ values. Overall, Island Queen has isotopically lighter and more heterogeneous magnetite compared to Tibes and Keystone. The $\delta^{56}Fe$ values are consistent with data from other Fe skarns. (Data compiled from: Wang et al., 2011; Zhu et al., 2020; Barefoot, 2021; Patrick, 2023; this study. Magnetite magmatic range after Heimann et al., 2008; Bilenker et al., 2016.)

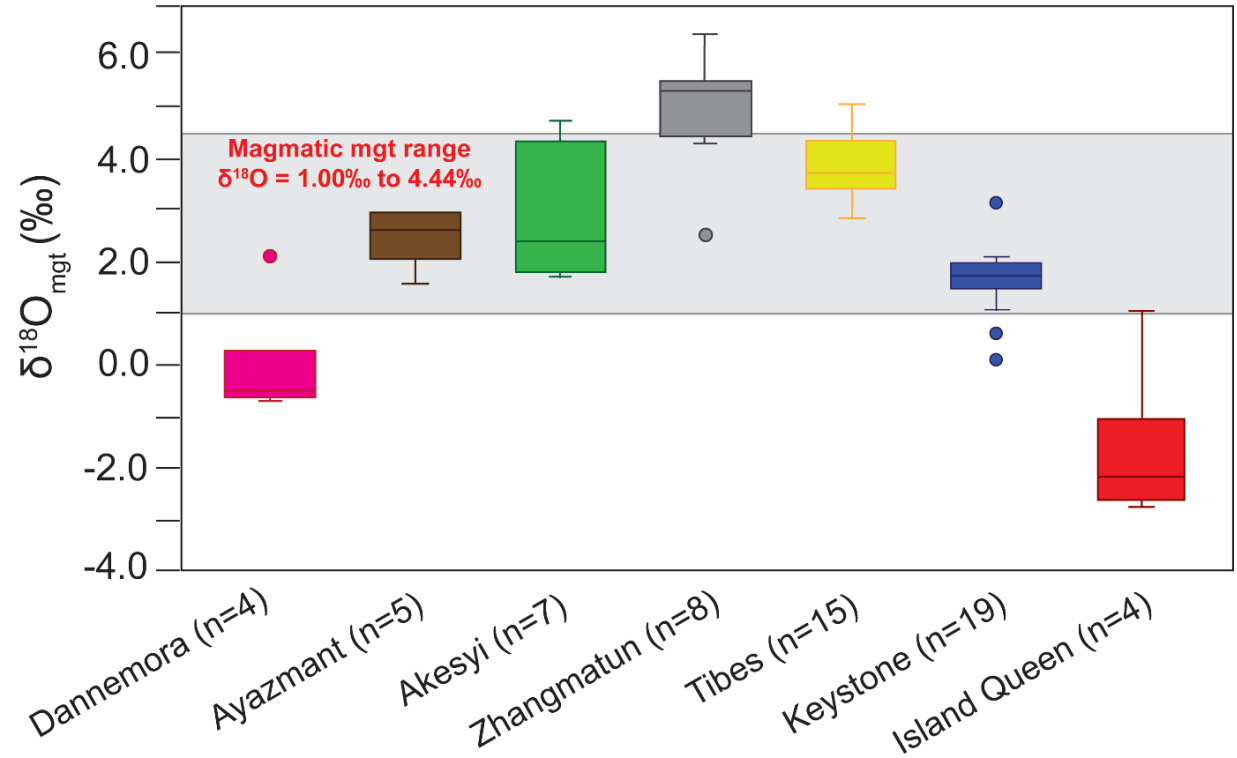

Figure 18. $\delta^{18}O$ values of Island Queen magnetite (mgt) compared to six global Fe-associated skarns. Dannemore and Ayazmant are Fe-Cu skarns, while the rest are Fe skarns. The magmatic range of magnetite is indicated by the grey box (Taylor, 1968). (Data compiled from: Troll et al., 2019, Oyman, 2010, Dong et al., 2021, Xie et al., 2017, Barefoot, 2021, and Patrick, 2023.)

7.5. Field accessibility of Puerto Rican Skarns

Island Queen, Keystone, and Tibes have varying degrees of accessibility and exposure (Table 5). This study determined that the Island Queen skarn is no longer reliably accessible in the field. Keystone, however, has an exposed magnetite ridge that is accessible, and the skarn extends to a neighboring hill, although the ridge is located on private property (Patrick, 2023). Tibes has the greatest exposure and is accessible to the public. Exposed by the Río Portugués, its 16 massive magnetite bodies can be mapped over a short distance in relation to the diorite stock (Barefoot, 2021; Giovannetti-Nazario, 2022). USGS Earth MRI efforts have gathered aeromagnetic data during geophysical fly overs of Puerto Rico, although the data set is not yet released. Ground-truthing these future maps will be crucial, and the more accessible outcrops

(Tibes and Keystone) should be targeted since they are well-characterized and exposed in the field. Like Island Queen, Keystone is hosted in weakly magnetic volcaniclastic rocks, which may complication the interpretation of aeromagnetic results. This information could then be used to interpret the aeromagnetic data for the Island Queen area in order to map the extent of this inaccessible deposit.

8. Future work and limitations of the study

The main limitation of this study is the poor accessibility of the outcrops. This study has defined the accessible portion of the Island Queen skarn ore and host rock, and the recovered magnetite samples record a clear source(s) of fluid and element mobility. For the first time, the Island Queen magnetite ore has been characterized in detail, and trace element and stable isotope compositions have been measured, providing new insights into an already limited database of Fe skarn studies. However, without a record of spatially constrained and/or mineralogically diverse samples, it is not possible to track fluid pathways or mapping alterations.

Future work can be done on the samples already collected to better understand skarn system geochemistry. Additional O isotope values for all ore samples could be used to further refine the extent of meteoric fluid input and the role they played in the alteration and deposition of the Island Queen magnetite. The garnets found in IQ-01 and IQ-10 could also be used to constrain timing of deposition. These garnets are Ca-rich and zoned in Fe and Al. Additional work could be done to study the fluid evolution of the system using the zonation found (Figure 19).

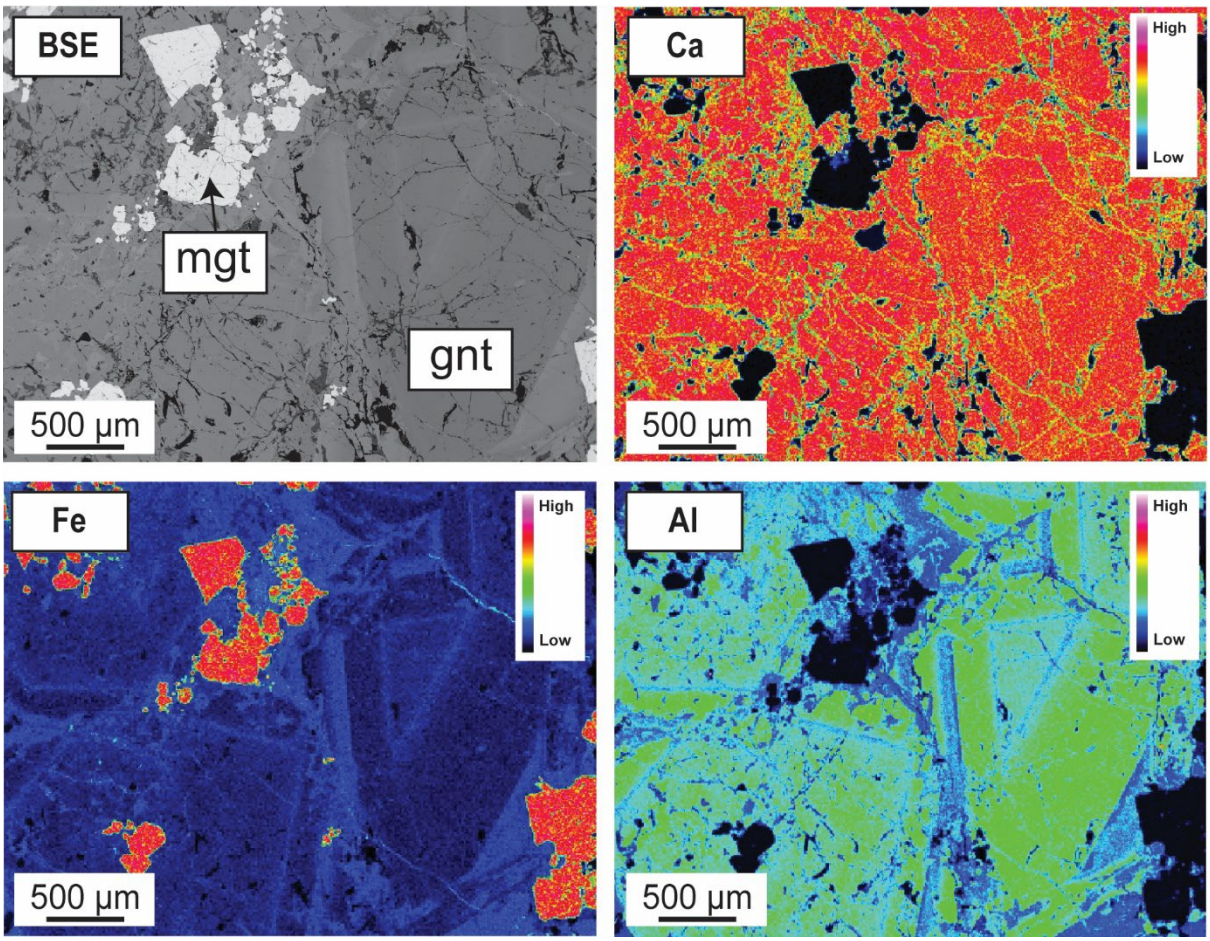

Figure 19. BSE image and EDS maps of IQ-10 garnet. The garnet is Ca-rich and zoned in trace amounts of Fe and Al. gnt= garnet, mgt = magnetite.

9. Conclusions

This study offers the first geochemical characterization of the Island Queen skarn in Puerto Rico. Field work documented an obscured Fe deposit and petrographic and geochemical methods thoroughly characterized the magnetite ore of the skarn and its limestone and volcaniclastic host rocks. The main conclusions of this study are:

- The Island Queen ore mineralogy consists mainly of magnetite that is altered to varying degrees to martite, hematite, goethite, and limonite. Dissolution-reprecipitation processes are recorded in the microscopic textures of the magnetite ore.
- The elemental and stable isotopic (Fe, O) compositions of Island Queen magnetite are consistent with global skarn deposits and reflects a high contribution of meteoric fluids during skarn formation.
- The ore geochemistry also reflects varied extents of interaction between the skarn fluids and limestone host rocks.
- Island Queen magnetite is geochemically zoned in Fe and Si, which is consistent with two other well-studied Puerto Rican Fe skarns, Tibes and Keystone.

To date, global Fe skarn studies have all been conducted on previously accreted Fe skarns. The characterization of the Fe ore at Island Queen contributes more data to the small global Fe skarn dataset and provides a rare look into the geochemistry of an unaccreted Fe skarn. Unfortunately, the Island Queen skarn is no longer accessible in the field, but this work can be used to understand Fe transport and deposition in skarn deposits on a global scale.

References

Barefoot, M. (2021). The Formation of Iron Ore at the Keystone Skarn, Puerto Rico. Master's Thesis, Auburn University.

Bawiec, W. J., Alonzo, R., Cox, D., Griscom, A., Lipin, B., Marsh, S., McKelvey, G., Page, N., & Schellekens, J. H. (1999). Mineral Resource Assessment of Puerto Rico. In Geology, geochemistry, geophysics, mineral occurrences and mineral resource assessment of the Commonwealth of Puerto Rico. U.S Geological Survey Open-File Report 98-38.

Bawiec, W. J., Cox, D., McKelvey, G., Griscom, A., & Marsh, S. (2001). Mineral Deposit Summary Sheets. In Geology, geochemistry, geophysics, mineral occurrences and mineral resource assessment of the Commonwealth of Puerto Rico. U.S Geological Survey Open-File Report 98-38.

Bilenker, L. D., Simon, A. C., Reich, M., Lundstrom, C. C., Gajos, N., Bindeman, I., Barra F., & Munizaga, R. (2016). Fe–O stable isotope pairs elucidate a high-temperature origin of Chilean iron oxide-apatite deposits. *Geochimica et Cosmochimica Acta*, 177, 94-104.

Bilenker, L. D., Weis, D., Scoates, J. S., & Perry, E. (2018). The application of stable Fe isotopes to magmatic sulfide systems: Constraints on the Fe isotope composition of magmatic pyrrhotite. *Economic Geology*, 113(5), 1181-1192.

Bindeman, I. (2008). Oxygen isotopes in mantle and crustal magmas as revealed by single crystal analysis. *Reviews in Mineralogy and Geochemistry*, 69, 445–478, https://doi.org/10.2138/rmg.2008.69.12.

Childress, T. M., Simon, A. C., Day, W. C., Lundstrom, C. C., & Bindeman, I. N. (2016). Iron and Oxygen Isotope Signatures of the Pea Ridge and Pilot Knob Magnetite-Apatite Deposits, Southeast Missouri, USA. In *Economic Geology* (Vol. 111, Issue 8, pp. 2033–2044), Society of Economic Geologists, https://doi.org/10.2113/econgeo.111.8.2033.

Childress T. M., Simon A. C., Reich M., Barra F., Bilenker L, D., La Cruz N. L., Bindeman I. N., Ovalle J. T. (2020). Triple Oxygen ($\delta^{18}O$, $\Delta^{17}O$), Hydrogen ($\delta^{2}H$), and Iron ($\delta^{56}Fe$) Stable Isotope Signatures Indicate a Silicate Magma Source and Magmatic-Hydrothermal Genesis for Magnetite Orebodies at El Laco, Chile. *Economic Geology*, 15 (7): 1519–1536, https://doi.org/10.5382/econgeo.4760.

Cox, D. & Briggs, R. (1973). Metallogenic Map of Puerto Rico (Ser. 721). U.S. Geological Survey.

Cooperman, A., Eberle A., Hettinger D., Marquis M., Smith B., Tusing R.F., Walzberg. J. (2023). Renewable Energy Materials Properties Database: Summary. National Renewable Energy Laboratory. NREL/TP-5000-82830. https://www.nrel.gov/docs/fy23osti/82830.pdf.

Dare, S. A., Barnes, S. J., Beaudoin, G., Méric, J., Boutroy, E., & Potvin-Doucet, C. (2014). Trace elements in magnetite as petrogenetic indicators. *Mineralium Deposita*, 49(7), 785-796.

Dupuis, C., & Beaudoin, G. (2011). Discriminant diagrams for iron oxide trace element fingerprinting of mineral deposit types. *Mineralium Deposita*, 46(4), 319-335.

Dong, R., Wang, H., Li, W., Yan, Q. H., & Zhang, X. (2021). The geology, magnetite geochemistry, and oxygen isotopic composition of the Akesayi skarn iron deposit, Western Kunlun Orogenic Belt, Xinjiang, northwest China: Implications for ore genesis. *Ore Geology Reviews*, 130, 103854, 1-19.

Einaudi, M. T., Meinert, L. D., & Newberry, R. J. (1981). Skarn deposits. *Economic Geology*, Seventy-Fifth Anniversary Volume, 317-391.

Heimann, A., Beard, B. L., & Johnson, C. M. (2008). The role of volatile exsolution and subsolidus fluid/rock interactions in producing high 56Fe/54Fe ratios in siliceous igneous rocks. *Geochimica et Cosmochimica Acta*, 72, 4379-4396.

Hu, H., Lentz, D., Li, J. W., McCarron, T., Zhao, X. F., & Hall, D. (2015). Reequilibration processes in magnetite from iron skarn deposits. Economic Geology, 110(1), 1-8.

Hu, X., Xiao, B., Jiang, H., Huang, J. (2023). Magnetite texture and trace element evolution in the Shaquanzi Fe-Cu deposit, Eastern Tianshan, NW China. *Ore Geology Reviews*, https://doi.org/10.1016/j.oregeorev.2023.105306.

Jolly, W. T., Lidiak, E. G., Schellekens, J. H., & Santos, H. (1998). Volcanism, tectonics, and stratigraphic correlations in Puerto Rico. In Special Paper of the Geological Society of America, Vol. 322, pp. 1–34, https://doi.org/10.1130/0-8137-2322-1.1.

King-Doonan, E. K., Bilenker L. D., Weis, D., Gordon, K., Fourny, A., Patton, G. M., Zhao, Y. (2024). A systematic investigation of the effects of the standard-sample concentration mismatch during Fe isotope measurement by MC-ICP-MS. *Geostandards and Geoanalytical Research*,48: 309-330, https://doi.org/10.1111/ggr.12541.

Knipping, J. L., Bilenker, L. D., Simon, A. C., Reich, M., Barra F., Deditius, A. P., Wälle, M., Heinrich, C. A., Holtz, F., Munizaga, R. (2015). Trace elements in magnetite from massive iron oxide-apatite deposits indicate a combined formation by igneous and magmatic-hydrothermal processes. *Geochimica et Cosmochimica Acta*, 171, 15-38.

Knoerr, A. W. (1952). Minnesota Mining Men Open up Rich Puerto Rico Iron Mine. *Journal of Minning Engineering,* 153, 74-9.

Krushensky, R., & Schellekens, J. H. (2001). Geology of Puerto Rico. In Geology, geochemistry, geophysics, mineral occurrences and mineral resource assessment of the Commonwealth of Puerto Rico (Open-File, pp. 25–40). U.S Geological Survey.

Lidiak, E. G., & Larue, D. K. (Eds.). (1998). Tectonics and geochemistry of the northeastern Caribbean. In Special Paper of the Geological Society of America, 322, V.

Masson, D. G., & Scanlon, K. M. (1991). The neotectonic setting of Puerto Rico. *Geological 28 Society of America Bulletin*, 103(1), 144–154.

Meinert, L. Dipple, G. & Nicolescu, S. (2005). World Skarn Deposits. Economic Geology 100th Anniversary Volume, 299-336.

M'Gonigle, J.M. (1978). Geologic Map of the Humacao Quadrangle, Puerto Rico. U.S. Geologic Survey.

Nadoll, P., Angerer, T., Mauk, J. L., French, D., & Walshe, J. (2014). The chemistry of hydrothermal magnetite: A review. *Ore Geology Reviews*, 61, 1-32.

Oyman, T. (2010). Geochemistry, mineralogy and genesis of the Ayazmant Fe–Cu skarn deposit in Ayvalik,(Balikesir), *Turkey. Ore Geology Reviews*, 37, 175-201.

Patrick, J. (2023). Developing a Genetic Model for Puerto Rico's Tibes Iron Deposit through Field Observations and Geochemical Analyses. Master's Thesis, Auburn University.

Pujols, E., & Cavosie, A. (2007). Geologic relations along the Rio Portugues near the Tibes stock contact aureole. [Unpublished Undergraduate Research]. University of Puerto Rico, Mayaguëz

Robb, L. (2005). Introduction to ore-forming processes. John Wiley & Sons.

Rodriguez-Mustafa, M. A., Simon, A. C., del Real, I., Thompson, J. F. H., Bilenker, L. D., Barra, F., Bindeman, I., & Cadwell, D. (2020). A Continuum from Iron Oxide Copper-Gold to Iron Oxide-Apatite Deposits: Evidence from Fe and O Stable Isotopes and Trace Element Chemistry of Magnetite. In *Economic Geology* (Vol. 115, Issue 7, pp. 1443–1459), Society of Economic Geologists, https://doi.org/10.5382/econgeo.4752

Schellekens, J. H. (1998). Geochemical evolution and tectonic history of Puerto Rico. In Special Paper of the Geological Society of America (Vol. 322), https://doi.org/10.1130/0-8137-2322-1.35.

Simon, A. C., Knipping, J., Reich, M., Barra, F., Deditius, A. P., Bilenker, L., & Childress, T. (2018). Kiruna-type iron oxide-apatite (IOA) and iron oxide copper-gold (IOCG) deposits form by a combination of igneous and magmatic-hydrothermal processes: evidence from the Chilean Iron Belt. *Economic Geology*, Special Publication, 21, 89-114

Tan W., Liu P., He H., Wang C., LiangX. (2016). Mineralogy and Origin of Exsolution in Ti-rich Magnetite from Different Magmatic Fe-ti Oxide-bearing Intrusions. *The Canadian Mineralogist*. V54 (3): 539–553. doi: https://doi.org/10.3749/canmin.1400069

Taylor, H. P. (1968). The oxygen isotope geochemistry of igneous rocks. *Contributions to Mineralogy and Petrology*, 19, 1-71, https://doi.org/10.1007/BF00371729.

Troll, V. R., Weis, F. A., Jonsson, E., Andersson, U. B., Majidi, S. A., Hogdahl, K., Harric, C., Millet, M., Chinnasamy, S. S., Kooijman, E., & Nilsson, K. P. (2019) Global Fe-O isotope correlation reveals magmatic origin of Kiruna-type apatite-iron-oxide ores. *Nature Communications*, 10, 1712, 1-12, https://doi.org/10.1038/s41467-019-09244-4.

Vazquez, L. (1960). Geology and ore deposits of the Keystone iron mine near Juncos, Puerto Rico. Department of Industrial Research, Economic Development Administration, Bulletin 7.

Wang, Y., Zhu, X. K., Mao, J. W., Li, Z. H., & Cheng, Y. B. (2011) Iron isotope fractionation during skarn-type metallogeny: a case study of Xinqiao Cu-S-Fe-Au deposit in the Middle-Lower Yangtze valley. *Ore Geology Reviews*, 43(1), 194-202.

Wawryk, C. M. & Foden, J. D. (2017). Iron-isotope systematics from the Batu Hijau Cu-Au deposit, Sumbawa, Indonesia. *Chemical Geology,* 466, 159–172, https://doi.org/10.1016/j.chemgeo.2017.06.004.

Weis, F. (2013). Oxygen and Iron Isotope Systematics of the Grängesberg Mining District (GMD), Central Sweden (Issue 251). University of Uppsala.

Wilburn, D.R. (2011). Wind energy in the United States and materials required for the land-based wind turbine industry from 2010 through 2030. U.S. Geological Survey Scientific Investigations Report. 2011–5036, 22. http://pubs.usgs.gov/sir/2011/5036

Xie, Q., Zhang, Z., Hou, T., Jin, Z., & Santosh, M. (2017). Geochemistry and oxygen isotope composition of magnetite from the Zhangmatun deposit, North China Craton: Implications for the magmatic-hydrothermal evolution of Cornwall-type iron mineralization. *Ore Geology Reviews*, 88, 57-70.

Yin, S., Wirth, R., He, H., Ma, C., Pan, J., Xing, J., Xu, J., Fu, J., & Zhang, X. N. (2021). Replacement of magnetite by hematite in hydrothermal systems: A refined redox-independent model. Earth and Planetary Science Letters, 577, 117-282.

Zhu, B., Zhang, H., Santosh, M., Su, B., Zhang, P., Han, C., & He, Y. (2020). Iron Isotopes Constrain the Metal Sources of Skarn Deposits: A Case Study from the Han-Zing Fe Deposit China. *Minerals*, 10(11), 951, 1-17.

Appendix A: Detailed geologic map of Puerto Rico

Map from Jolly et al., 1998 showing the geologic units and fault traces within the three igneous provinces (also known as the Southwestern Igneous Province, Central Igneous Province, and Northeastern Igneous Province; see Figure 2).

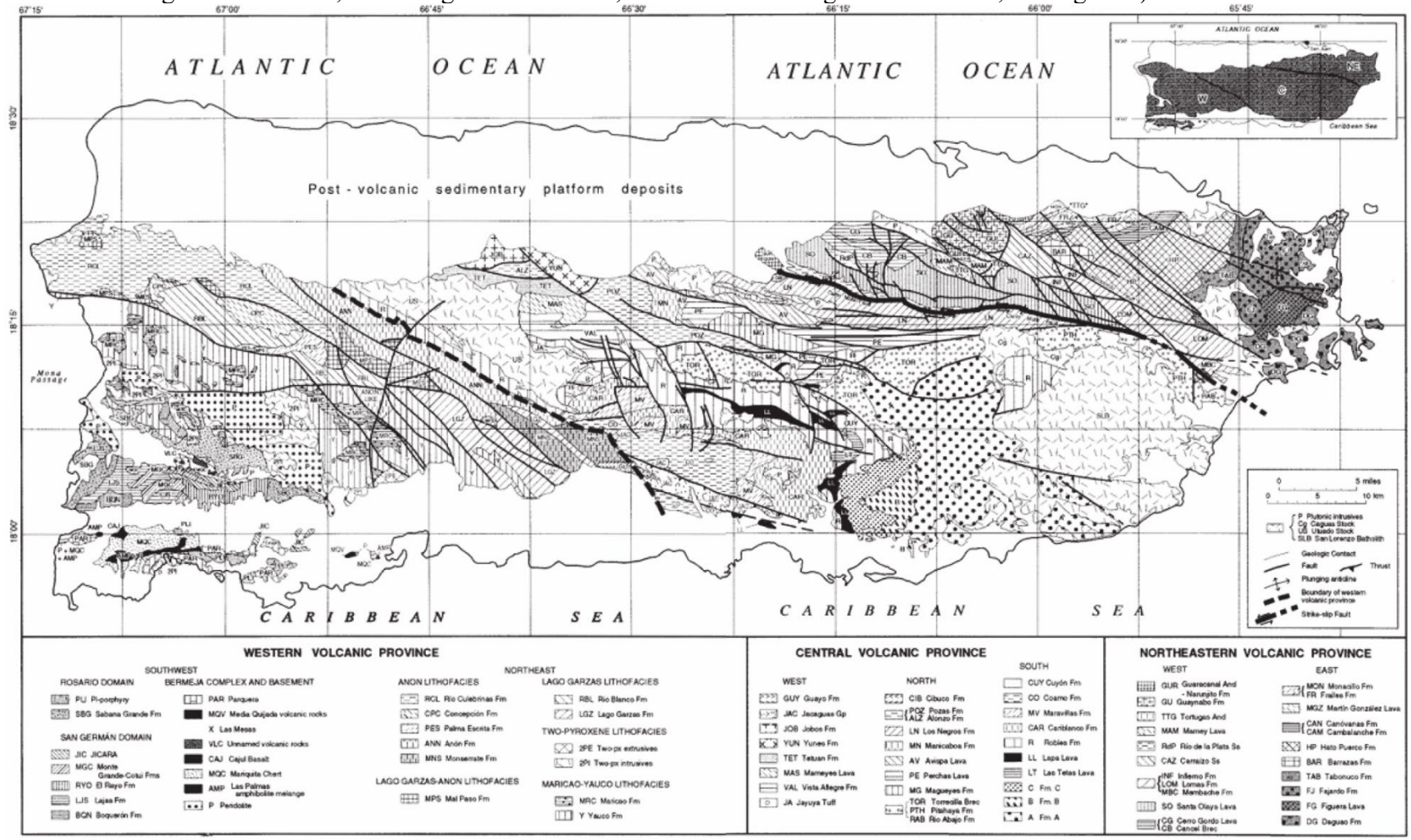

Appendix B: Full list of FeO wt% totals measured by EPMA.

FeO wt% total values measured using EPMA, FeO is computer optimized to balance FeO and Fe_2O_3. Mgt = magnetite spots that are not associated with a LA-ICP-MS spot, LA = magnetite spots that are associated with corresponding LA-ICP-MS spots, and hem = hematite spot analysis.

Sample	FeO wt% (T)*
IQ01-mgt1	88.91
IQ01-mgt2	89.15
IQ01-mgt3	93.36
IQ01-mgt4	93.95
IQ01-mgt5	92.86
IQ02-LA1	89.67
IQ02-LA2	91.36
IQ02-LA3	89.44
IQ02-LA4	89.10
IQ02-LA5	90.59
IQ02-LA6	89.19
IQ02-LA7	91.13
IQ02-LA8	89.84
IQ03-LA00	90.02
IQ03-LA01	87.73
IQ03-LA02	87.50
IQ03-LA03	89.64
IQ04-LA1	87.80
IQ04-LA2	90.02
IQ04-LA3	87.73
IQ04-LA4	87.50
IQ04-mgt	89.64
IQ04-hem-1	3.00
IQ04-hem-2	88.66
IQ04-hem-3	86.53
IQ05-LA1	88.70
IQ05-LA2	86.26
IQ05-LA3	89.68
IQ05-LA4	86.07
IQ05-LA5	87.80

Sample	FeO wt% (T)*
IQ05-mgt-1	88.27
IQ05-mgt-2	90.37
IQ05-mgt-3	84.80
IQ05-mgt-4	87.03
IQ08-LA1	89.58
IQ08-LA4	88.70
IQ08-LA2	90.43
IQ08-LA3	92.08
IQ08-LA5	90.92
IQ08-red-1	73.24
IQ08-mgt-1	91.08
IQ08-mgt-2	91.13
IQ08-mgt-3	90.09
IQ09-LA1	91.07
IQ09-LA2	89.65
IQ09-LA3	85.45
IQ09-LA4	86.32
IQ09-LA5	91.78
IQ10-LA1	92.24
IQ10-LA2	92.15
IQ10-LA3	94.05
IQ10-LA4	93.23
IQ10-LA5	93.27
IQ15-LA1	91.85
IQ15-LA2	90.92
IQ15-LA3	93.19
IQ15-LA4	87.72
IQ15-LA5	81.98
IQ15-LA6	89.14
IQ15-LA7	91.28
IQ15-LA8	91.52

Appendix C: Full list of trace element concentrations measured with LA-ICP-MS

Trace element concentrations (ppm) of the magnetite ore samples measures by LA-ICP-MS. Blank cells = element concentrations that were not analyzed for that sample.

Sample	^{23}Na	^{24}Mg	^{25}Mg	^{27}Al	^{29}Si	^{43}Ca	^{44}Ca	^{47}Ti	^{51}V	^{52}Cr	^{55}Mn	^{59}Co	^{Ni}60	^{63}Cu	^{66}Zn	^{71}Ga	^{118}Sn
IQ01 spot4		323.3	326.1	1641.5	5954.6	1836.7	1758.7	762.2	231.2	49.1	2119.4	97.6	168.9			3.1	
IQ01 spot5		321.8	317.3	951.7	5532.9	1215.3	1217.9	275.1	184.0	29.4	2441.2	93.7	184.8			3.3	
IQ01 spot6		308.5	316.4	1068.3	7883.0	563.1	649.5	719.1	36.4	0.0	2652.4	89.4	33.7			2.5	
IQ01 spot7		243.9	239.1	916.7	7547.3	593.4	534.2	788.5	120.8	9.2	2647.7	80.0	45.9			2.5	
IQ01 spot8		54.4	53.5	333.2	1803.7	411.5	562.6	215.6	108.5	11.4	2117.4	88.3	127.7			2.2	
IQ02_LA1	60.8	40.5	41.3	1266.4	2688.7	61.6	55.6	164.7	74.5	0.2	2030.0	157.3	1.2	36.7	670.6	5.8	0.2
IQ02_LA2	30.8	42.7	42.0	977.1	2580.6	69.8	95.5	405.8	78.8	4.3	1985.8	165.4	0.7	39.5	499.2	5.4	0.2
IQ02_LA3	251.9	407.8	417.5	1703.2	14066.4	1607.8	1721.8	397.3	21.6	18.5	2163.0	168.0	3.6	0.0	103.0	8.1	0.2
IQ02_LA4	45.7	67.7	67.7	2310.4	3743.5	98.3	107.1	226.5	102.7	0.8	1686.6	192.4	1.5	99.5	857.6	8.1	0.4
IQ02_LA5	42.2	150.5	153.0	1746.6	5183.4	60.7	111.4	271.1	87.0	1.7	1868.8	150.0	1.8	142.0	548.1	5.8	0.2
IQ02_LA6	358.3	1886.7	1877.3	5326.4	77020.8	5072.1	5577.6	591.2	78.8	128.4	2897.4	180.5	5.4	8.7	194.7	13.0	0.2
IQ02_LA7	20.7	67.2	67.8	208.1	7151.9	152.5	155.0	99.3	19.7	0.7	1477.2	155.2	4.4	0.0	46.8	4.2	0.1
IQ02_LA8	29.0	43.1	44.0	2911.7	3041.5	86.7	78.3	51.9	55.6	1.1	1935.5	176.4	2.1	53.5	1680.0	7.4	0.1
IQ03 spot2		1514.0	1636.9	3813.0	15243.9	1674.1	133.8	269.9	104.7	112.2	829.9	103.2	7.0			5.9	
IQ03 spot5		968.6	1022.6	3199.2	15601.1	948.2	908.3	334.4	104.6	54.0	870.8	105.5	8.4			5.3	
IQ04-LA1	335.2	348.2	350.8	3047.3	13564.7	1674.3	1736.0	3702.4	299.7	34.9	1243.3	68.5	9.6	193.9	312.5	5.8	0.7
IQ04-LA2	620.1	440.4	435.2	4984.2	18632.9	3406.4	3652.9	240.5	99.6	1.5	2530.1	66.5	6.3	114.5	369.7	8.5	0.2
IQ04-LA3	412.1	385.0	385.7	2377.7	18039.2	1884.4	1987.8	37.6	69.7	0.7	1599.0	61.3	8.0	41.1	176.5	6.1	0.1
IQ04-LA4	253.7	177.0	185.3	2061.5	9872.3	868.0	968.0	3302.6	374.1	132.4	991.5	60.0	12.8	119.0	499.1	7.7	0.8
IQ04-LA5	303.8	248.0	247.4	1650.8	13315.5	1273.3	1370.8	30.8	56.9	0.9	1420.6	63.9	9.6	91.0	362.7	6.1	0.6
IQ05-LA1	228.3	601.8	580.0	2211.2	20779.4	1128.7	1269.0	145.8	49.5	2.0	1547.3	58.8	6.5	76.8	315.2	4.5	0.2
IQ05-LA2	248.4	674.5	660.0	2133.4	24911.5	1346.4	1389.7	91.4	17.5	0.7	1893.9	65.4	4.9	24.2	159.3	4.8	0.2
IQ05-LA3	72.6	497.1	490.3	1830.3	17708.2	322.9	375.0	57.6	73.1	5.8	950.3	65.0	8.5	139.2	198.8	3.8	0.2
IQ05-LA4	358.7	301.8	297.0	2343.8	18218.1	2109.0	2253.1	133.4	116.0	1.6	1424.0	66.3	6.1	77.3	255.5	5.2	0.4
IQ05-LA5	179.0	471.9	464.4	1528.0	20492.1	754.0	780.2	85.5	33.0	8.1	1422.0	60.9	5.3	10.2	114.6	4.1	0.1

Sample	^{23}Na	^{24}Mg	^{25}Mg	^{27}Al	^{29}Si	^{43}Ca	^{44}Ca	^{47}Ti	^{51}V	^{52}Cr	^{55}Mn	^{59}Co	^{Ni}60	^{63}Cu	^{66}Zn	^{71}Ga	^{118}Sn
IQ08-LA1	105.0	164.1	161.9	916.7	9948.9	557.4	580.2	154.4	35.5	0.5	2574.3	86.4	4.9	64.7	374.9	2.4	0.4
IQ08-LA2	189.9	228.0	229.7	1461.9	11789.0	1253.4	1230.2	300.3	69.3	36.9	3185.2	94.0	5.9	28.1	184.0	3.4	0.1
IQ08-LA3	192.9	265.0	257.7	1736.8	13253.6	857.3	1017.7	225.9	30.5	0.1	2964.1	82.8	4.8	70.9	796.8	3.2	0.0
IQ08-LA4	114.9	142.4	138.1	900.7	9178.5	693.0	754.8	267.5	27.4	2.3	2815.4	90.5	5.2	14.8	95.3	2.5	0.1
IQ08-LA5	322.5	329.7	328.4	1901.5	13221.6	2273.9	2305.7	415.4	52.2	0.9	3972.9	92.0	5.2	7.6	122.4	3.8	0.1
IQ09-LA1	17.1	1178.0	1125.4	3205.3	4361.2	130.2	113.4	56054.1	2093.5	359.6	666.3	126.8	89.8	26.8	210.7	4.1	1.8
IQ09-LA2	792.0	1677.7	1657.6	8091.4	20918.4	4270.7	4531.5	1937.5	92.3	14.0	1382.9	146.6	7.7	6.0	278.9	12.4	0.1
IQ09-LA3	1540.0	1555.5	1520.6	12297.4	29499.4	7671.6	7993.0	2412.8	202.4	28.6	1855.6	152.3	18.8	54.3	432.5	20.2	0.1
IQ09-LA4	947.5	1115.1	1105.0	7928.5	21484.2	4360.2	4775.7	1293.9	243.5	34.5	1325.3	151.3	19.3	176.8	387.7	13.1	0.1
IQ09-LA5	8.7	115.4	108.7	634.7	1298.6	41.7	73.6	22786.7	2416.0	298.3	503.9	114.1	149.5	6.9	121.2	3.4	0.4
IQ10-LA1	12.8	303.3	297.9	2423.8	1224.8	58.9	66.4	794.6	245.2	0.9	1911.6	74.5	264.9	0.1	1455.9	8.3	0.3
IQ10-LA2	29.1	587.4	602.4	2698.1	1683.5	177.4	194.4	306.1	230.8	5.8	1598.2	73.2	235.9	0.0	979.0	9.4	0.2
IQ10-LA3	61.3	538.9	519.5	2579.9	2139.9	335.6	401.9	307.8	217.7	10.5	1611.1	70.9	220.7	0.8	906.7	10.6	1.8
IQ10-LA4	87.7	500.6	467.0	1797.6	1982.9	247.9	288.9	577.3	284.1	28.3	1659.6	79.1	268.9	0.9	952.8	7.0	3.4
IQ10-LA5	85.5	594.7	587.0	2642.5	2265.0	402.7	476.6	743.0	260.4	18.8	2036.6	84.7	268.5	0.0	1262.3	7.2	0.4
IQ15_LA1	118.6	6317.0	6244.5	17882.7	35754.6	225.6	217.1	194.8	62.1	0.7	1577.9	129.9	11.1	55.0	1294.5	15.4	0.0
IQ15_LA2	94.2	202.6	204.1	608.9	14545.8	205.7	223.4	39.4	25.8	11.9	518.6	73.8	4.9	13.8	164.2	5.8	0.2
IQ15_LA3	138.4	2374.5	2335.2	6244.2	23544.8	530.7	504.8	86.9	61.8	18.4	1060.4	106.7	9.4	173.3	1467.9	10.6	1.6
IQ15_LA4	103.8	320.8	315.8	757.3	14066.5	407.2	385.4	111.2	87.1	4.6	753.9	71.4	6.9	2.2	264.9	6.2	0.3
IQ15_LA5	136.3	202.1	211.1	560.2	8683.5	738.4	826.7	59.6	28.0	6.7	285.7	68.3	10.1	6.1	159.5	6.0	0.3
IQ15_LA6	129.3	281.0	279.5	1035.1	9315.2	385.8	398.4	87.6	78.4	3.2	465.0	75.8	7.6	380.6	1523.5	5.9	0.4
IQ15_LA7	45.5	120.7	126.9	1390.1	3326.4	376.8	568.3	100.9	60.8	3.1	306.0	89.0	5.3	86.1	657.3	6.0	0.6
IQ15_LA8	22.2	88.9	92.8	1668.8	1685.3	114.9	72.7	95.8	63.8	0.4	255.0	66.0	3.9	0.3	587.0	5.1	0.2

Appendix D: Complete set of Island Queen element maps from EPMA.

BSE and elemental maps from additional Island Queen ore samples. Color scale in the upper right corner is valid for all elemental maps and represents relative element concentrations.

IQ-03: magnetite

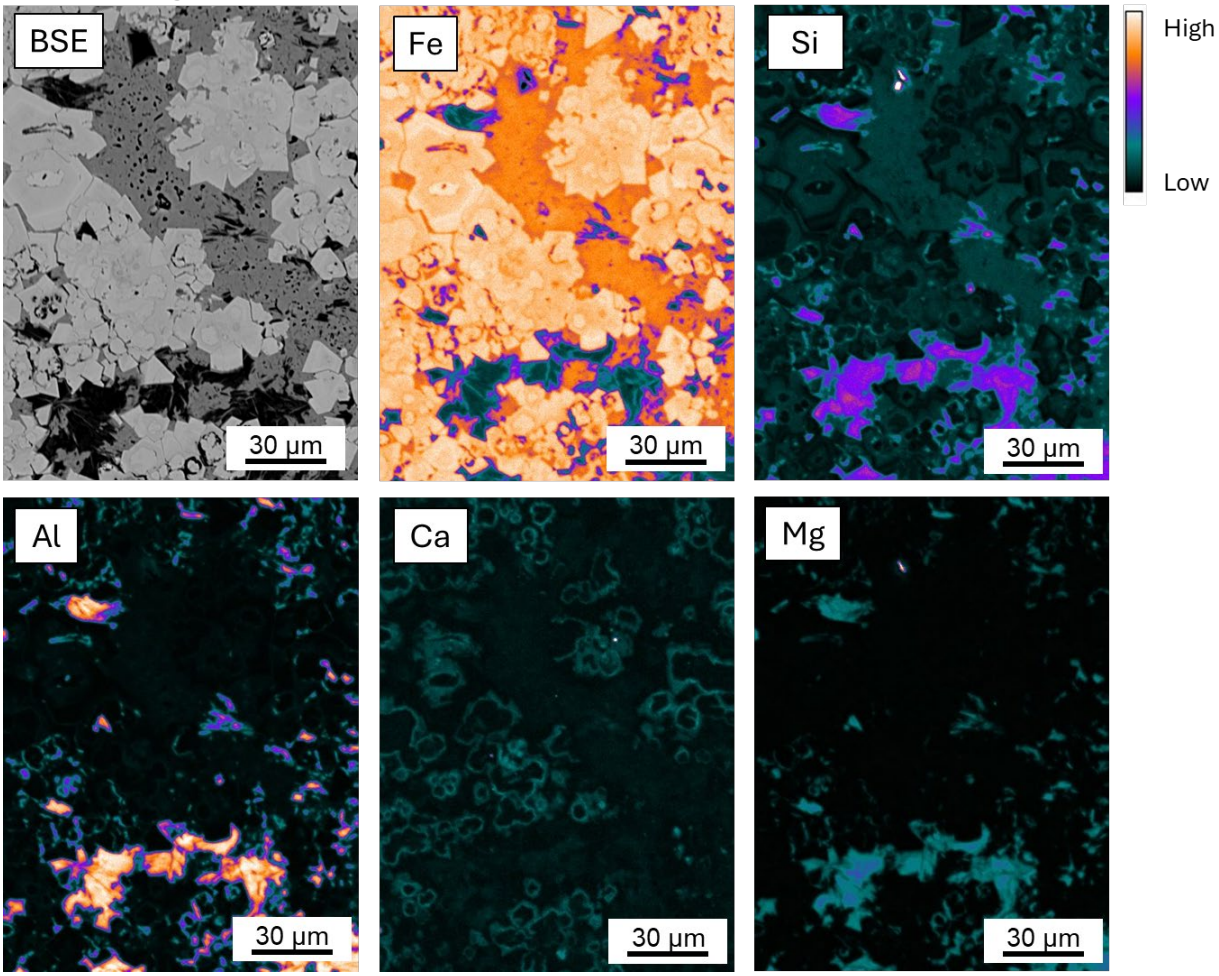

IQ-03: magnetite with Al-rich vein and rutile

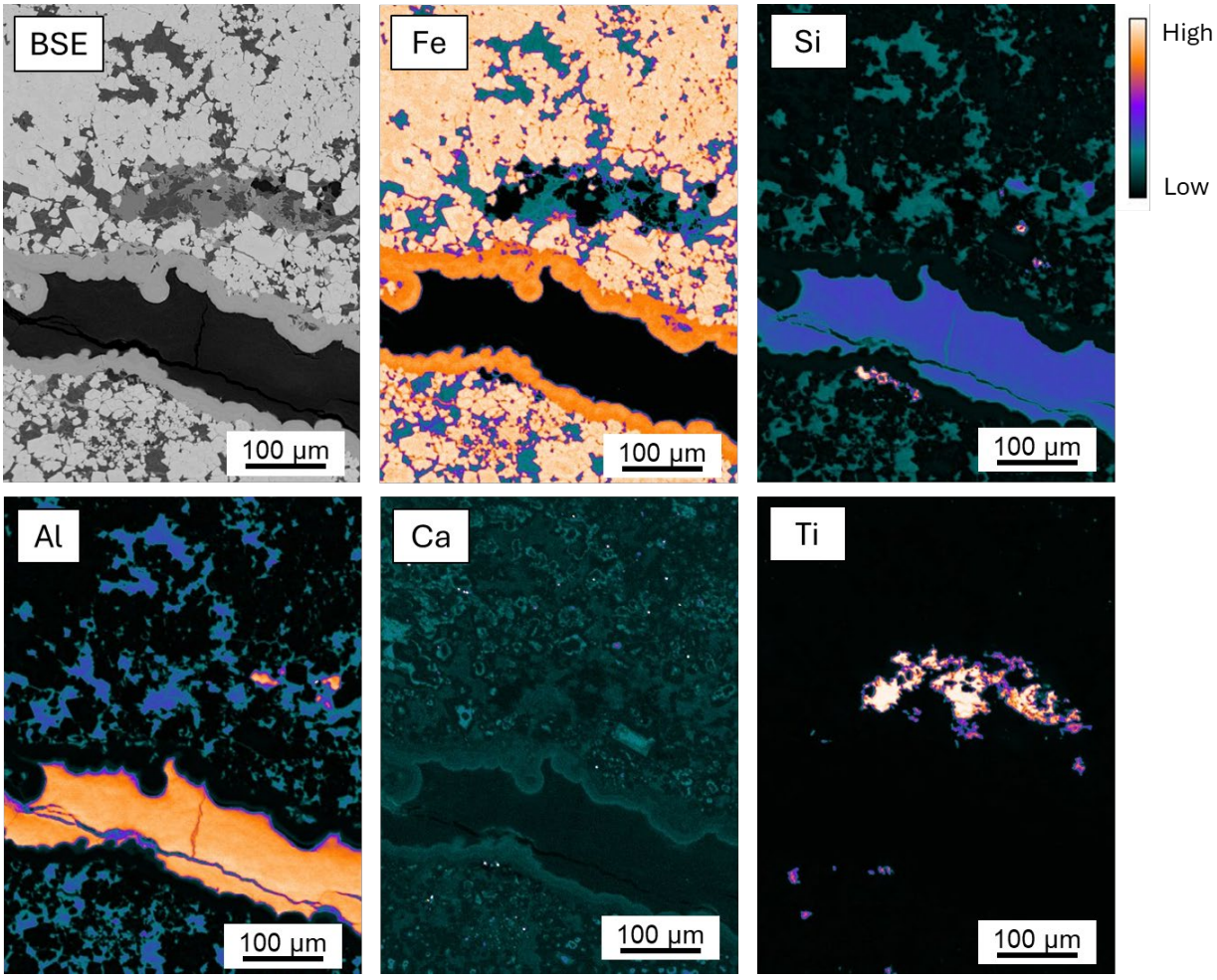

IQ-04: hematite surrounded by quartz

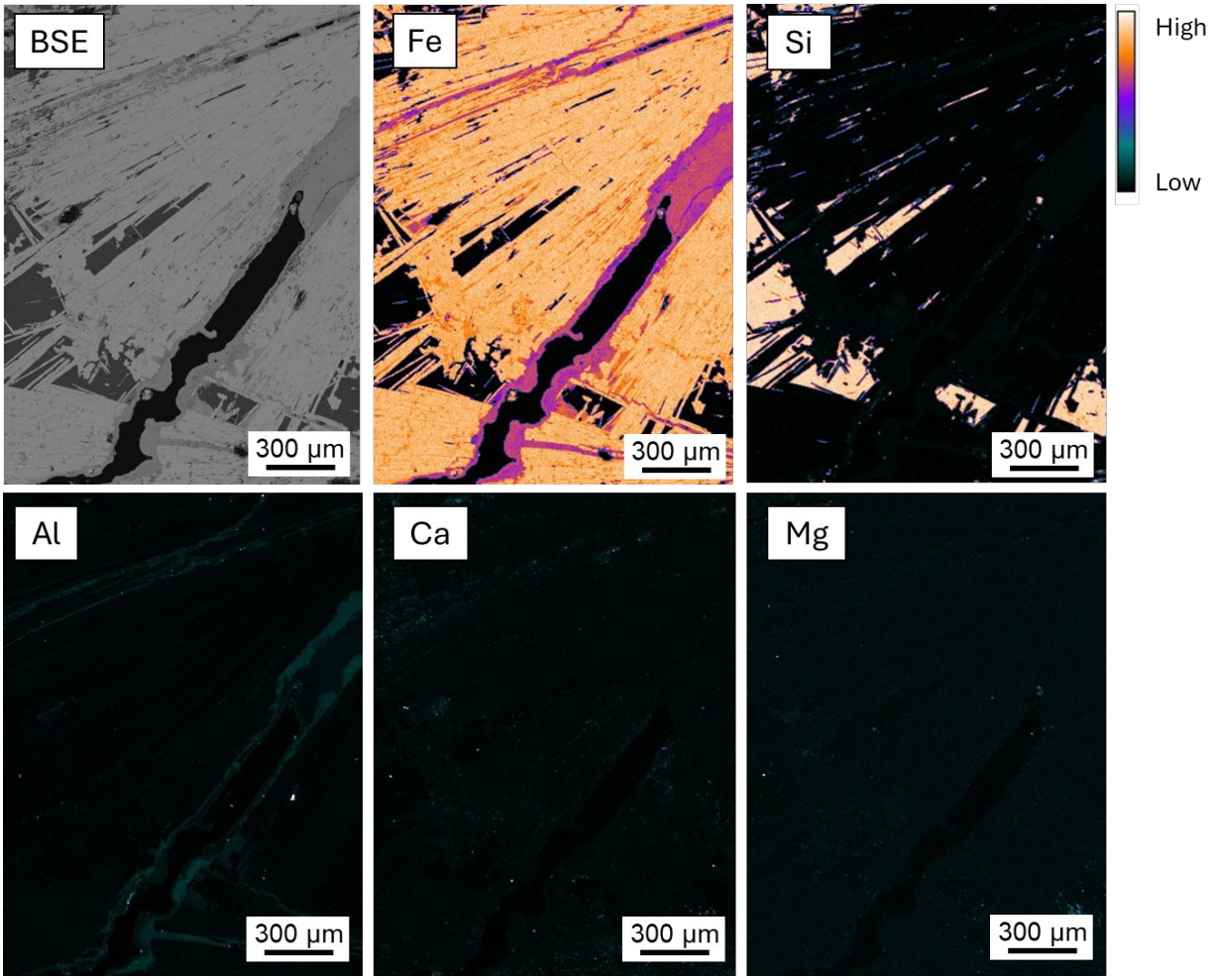

IQ-05: magnetite with dissolution-reprecipitation textures

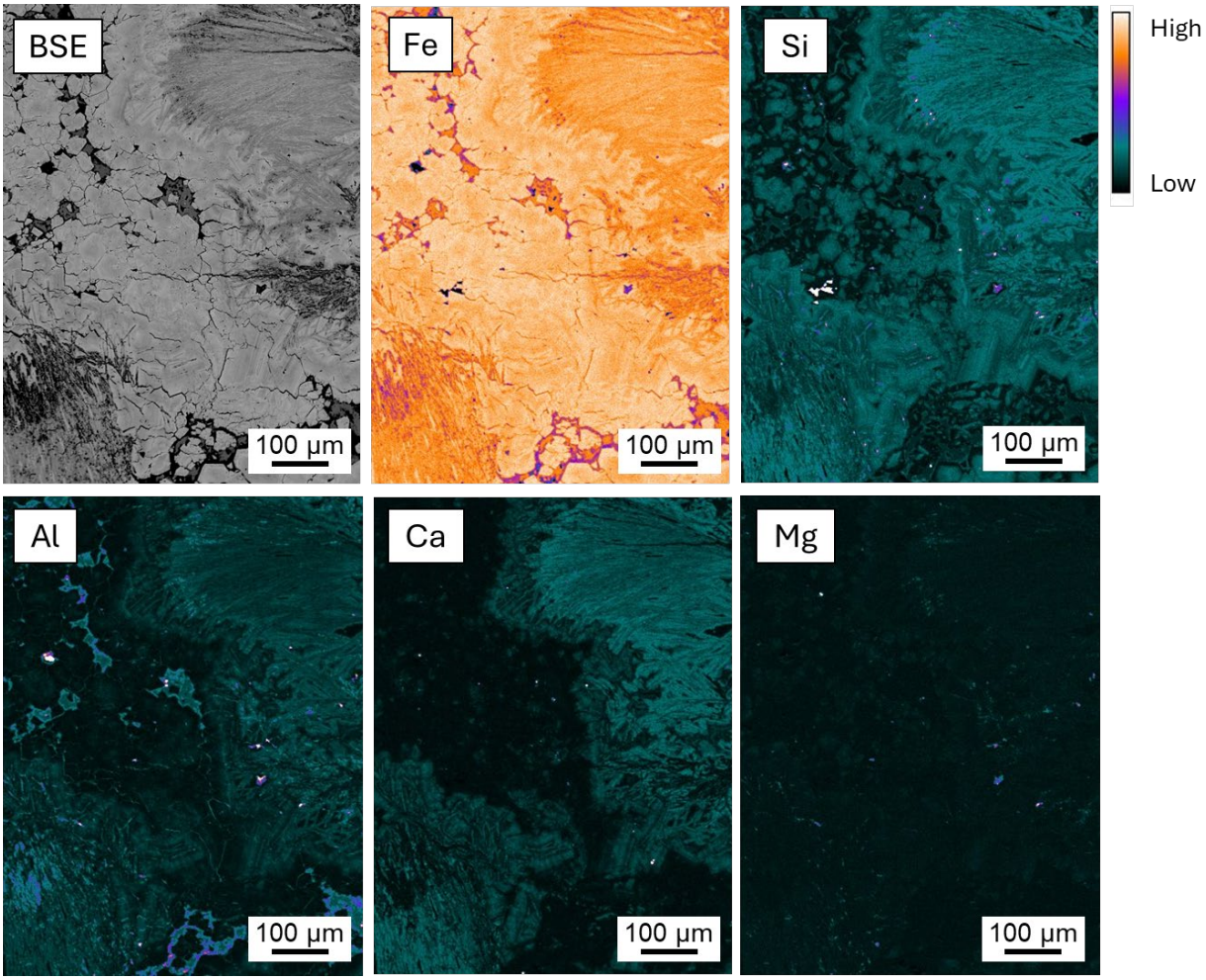

IQ-08: magnetite

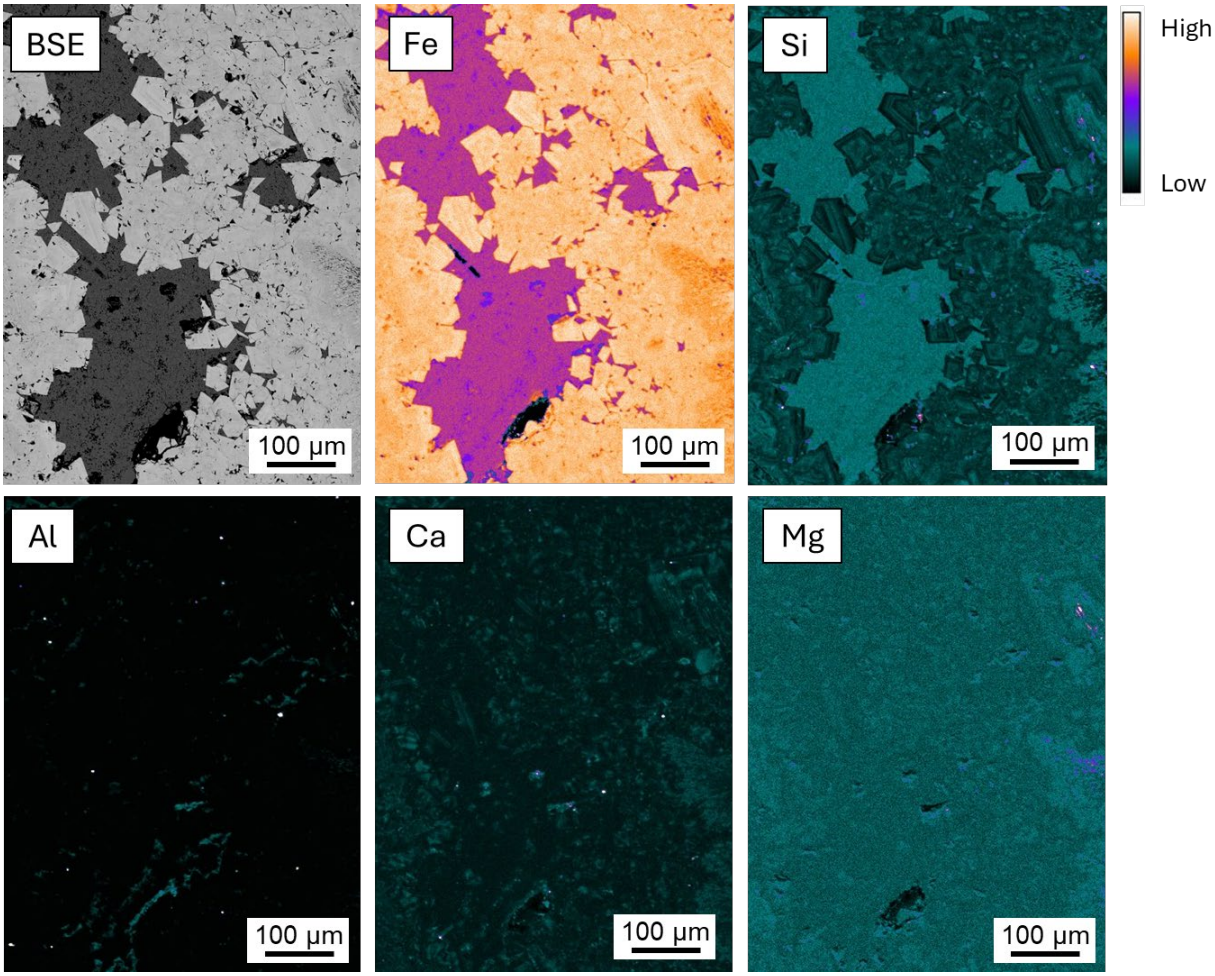

IQ-09: magnetite with ilmenite exsolution

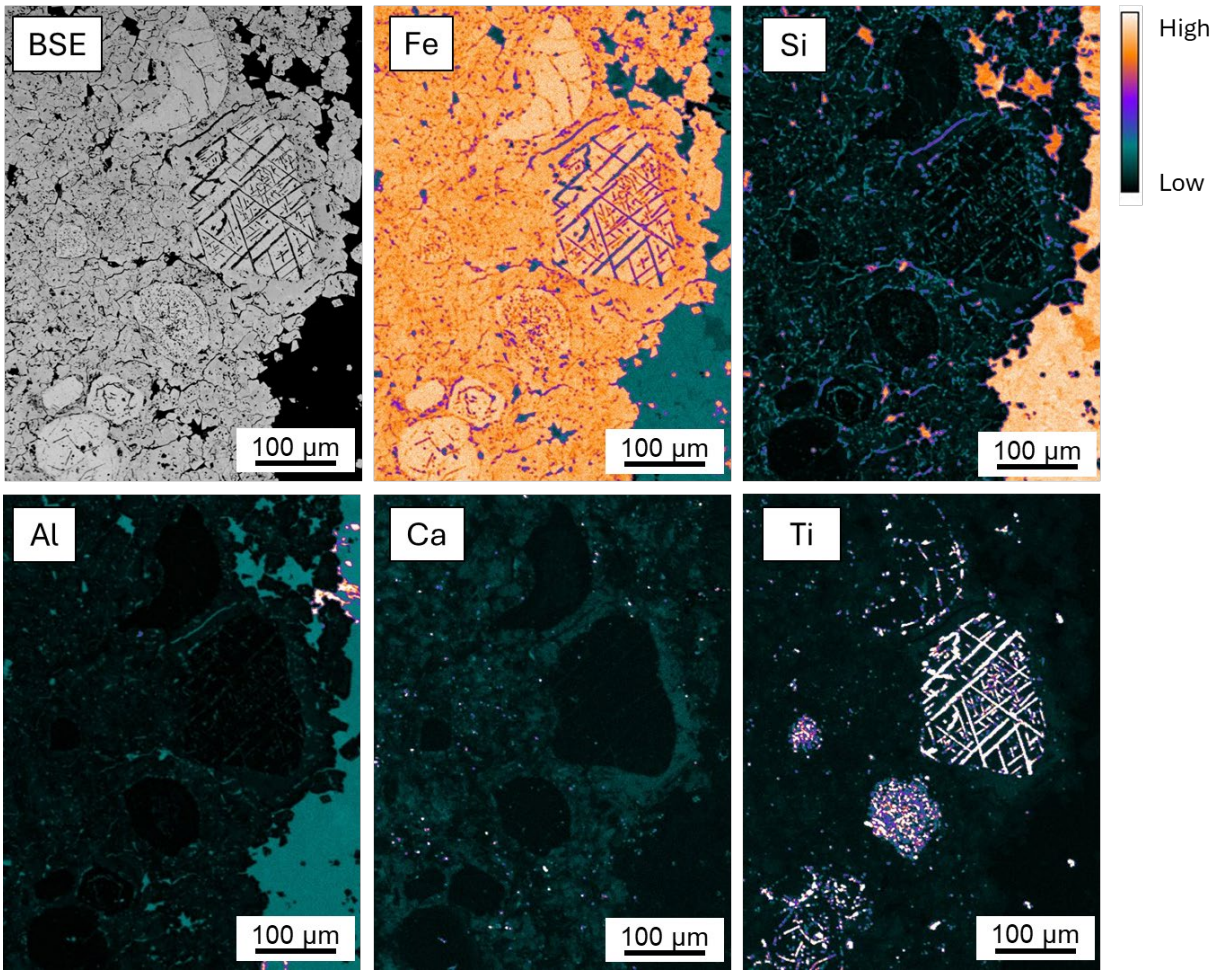

IQ-15: magnetite

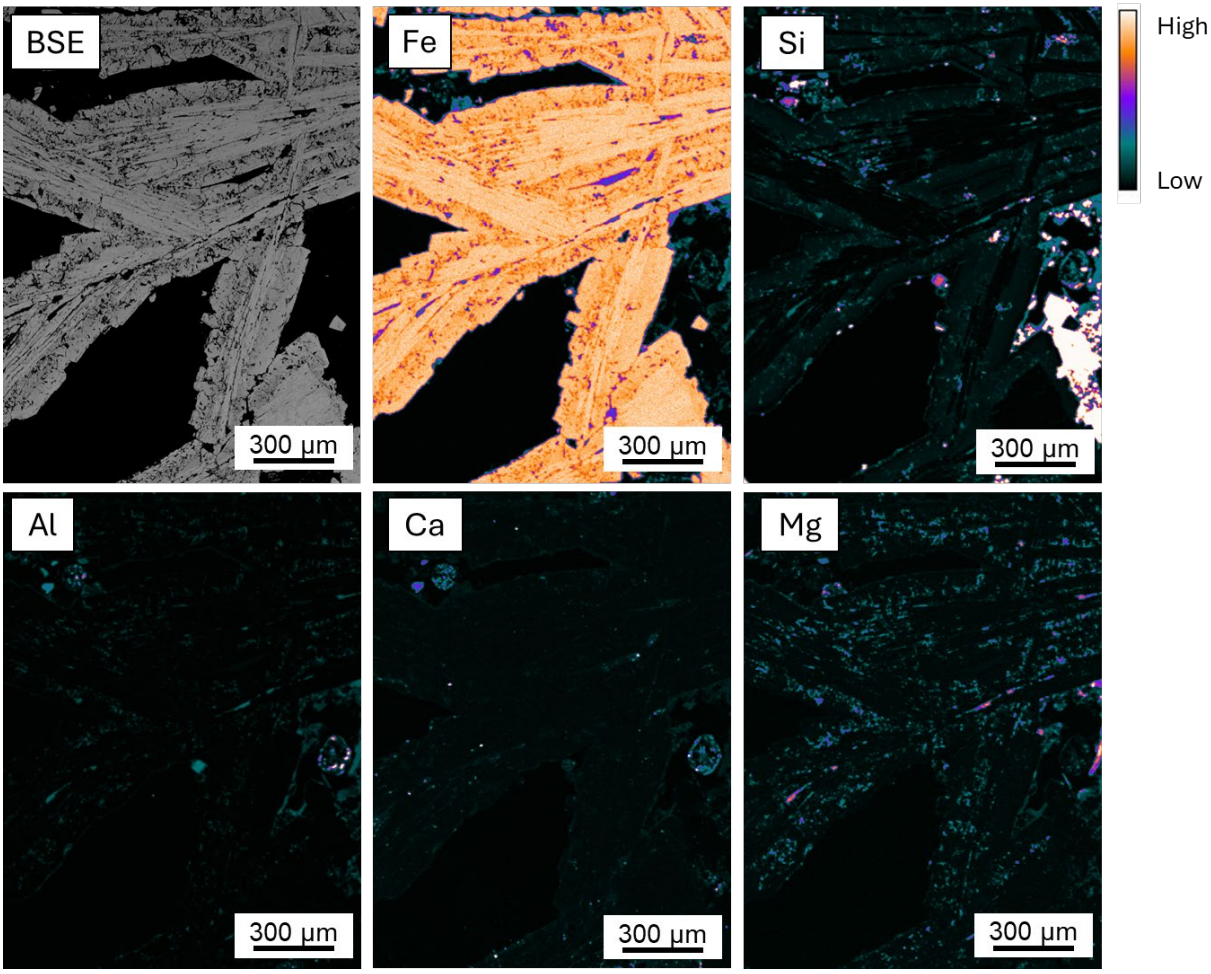

IQ-10: garnet surrounded by magnetite